NASA TM X-323

TECHNICAL MEMORANDUM

X-323

STABILITY AND CONTROL CHARACTERISTICS AT A MACH NUMBER OF 1.97 OF AN AIRPLANE CONFIGURATION HAVING TWO TYPES OF VARIABLE-SWEEP WINGS

By Gerald V. Foster and Odell A. Morris

Langley Research Center
Langley Field, Va.

NATIONAL AERONAUTICS AND SPACE ADMINISTRATION

WASHINGTON

August 1960

1S

NATIONAL AERONAUTICS AND SPACE ADMINISTRATION

TECHNICAL MEMORANDUM X-323

STABILITY AND CONTROL CHARACTERISTICS AT A MACH NUMBER OF 1.97 OF AN AIRPLANE CONFIGURATION HAVING TWO TYPES OF VARIABLE-SWEEP WINGS*

By Gerald V. Foster and Odell A. Morris

L
1
0
7
2

31731

SUMMARY

An investigation has been conducted in the Langley 4- by 4-foot supersonic pressure tunnel at a Mach number of 1.97 to determine the stability and control characteristics of an airplane configuration with two types of variable-sweep wings. The design of these wings differed primarily in the pivot location about which the wing sweep angle was varied. The pivot of one wing was located at approximately the 50-percent-semispan station; whereas, the pivot of the other wing was located within the body.

The configuration with the wing, body, and tails exhibited linear variation of pitching moment with lift coefficient, positive directional stability, and positive effective dihedral with either wing configuration.

These results, in conjunction with low-speed results for the same model obtained from NASA Technical Memorandum X-303, indicate that the total change in static margin due to increasing the Mach number and changing the wing sweep from 25° to 75° is about 18 percent of the mean geometric chord for the outboard-pivot configuration and about 26 percent for the inboard-pivot configuration for a sweep-angle variation from 30° to 70.5°.

INTRODUCTION

Recent studies of the use of variable wing sweep have indicated that such an arrangement might provide a satisfactory means of combining efficient subsonic and supersonic flight characteristics into one airplane. In comparison to conventional supersonic airplanes, a

[redacted]

variable-sweep wing with its high-aspect-ratio potential provides a means of reducing the take-off and landing distance and of increasing the subsonic range for ferrying missions. On the basis of previous results obtained at subsonic speeds (ref. 1) a configuration with a wing, body, and horizontal tail has been evolved which permitted large variations of the sweep angle of the outboard wing panels with a minimum of aerodynamic-center shift. The results of wind-tunnel studies of the stability and control characteristics of this configuration are presented in references 2 to 6 for a speed range up to a Mach number of 3.71. Further studies were conducted at subsonic speeds with a similar wing having an outboard-pivot location on a model more representative of current fighter aircraft and, in addition, with a more conventional wing having an inboard pivot located within the fuselage. (See ref. 7.)

The present paper presents results of an investigation at a Mach number of 1.97 of the models presented in reference 7 which include the two types of variable-wing-sweep designs, one having a pivot outboard on the wing and the other having a pivot located within the fuselage. The sweep angles of these wings were fixed, for the major portion of the investigation, at 75° for the outboard-pivot location and 70.5° for the inboard-pivot location.

A limited investigation has been conducted on the outboard-pivot wing design having a leading-edge sweep angle of 113°. This design may be considered as a possible low-altitude supersonic-attack configuration in which a major portion of the wing could be hidden within the fuselage in order to facilitate reduction in high dynamic pressure, gust-load acceleration, friction drag, and wave drag (ref. 8).

SYMBOLS

The results are referred to the body-axis system except for the lift and drag coefficients which are referred to the wind-axis system. The moment reference point for all configurations is located at 67.03 percent of the body length measured from the nose and 1.13 percent of the body length above the body reference line, corresponding to the moment reference of reference 7.

The coefficients of the various configurations are based on the geometry of the wing to which they apply except for the coefficients of the configuration incorporating the 113° sweptback wing which are based on those of the 75° sweptback wing.

C_L	lift coefficient, $\frac{\text{Lift}}{qS}$
C_D	drag coefficient, $\frac{\text{Drag}}{qS}$
C_m	pitching-moment coefficient, $\frac{\text{Pitching moment}}{qS\bar{c}}$
C_l	rolling-moment coefficient, $\frac{\text{Rolling moment}}{qSb}$
C_n	yawing-moment coefficient, $\frac{\text{Yawing moment}}{qSb}$
C_Y	side-force coefficient, $\frac{\text{Side force}}{qS}$
q	free-stream dynamic pressure, lb/sq ft
S	wing area, sq ft
$\bar{c}$	wing mean geometric chord, in.
b	wing span, in.
M	free-stream Mach number
α	angle of attack, deg
β	angle of sideslip, deg
δ_c	canard deflection, deg
δ_h	horizontal-tail deflection, deg
Γ	horizontal-tail dihedral angle, deg
Λ	leading-edge sweep angle, deg
L/D	lift-drag ratio, C_L/C_D
$(L/D)_{max}$	maximum lift-drag ratio

C_{n_β} directional-stability parameter, $\partial C_n/\partial\beta$

C_{l_β} effective-dihedral parameter, $\partial C_l/\partial\beta$

C_{Y_β} side-force parameter, $\partial C_Y/\partial\beta$

Components of model:

B body

H horizontal tail

V vertical tail

W wing

C canard

MODEL AND APPARATUS

Details of the models investigated are presented in figure 1, with photographs of the configurations presented in figures 2 and 3. The geometric characteristics of the models are presented in table I.

The two wings used in these tests are designated herein as wings 1 and 2. These wings differed primarily in the location of the pivot about which the wing sweep angle could theoretically be varied. The pivot of wing 1 (fig. 1(a)) was located outboard from the body at a spanwise station corresponding to 51.08 percent semispan of the wing; whereas the pivot of wing 2 was located within the body (fig. 1(b)). The leading-edge sweep angle of wing 1 was increased from 75° to 113° (fig. 1(c)) for a part of these tests and is designated herein as wing 3.

These wings were attached to the body in a high wing position with incidence and dihedral angles of 0°. The leading-edge control and spoiler-slot-deflector control shown on the wing 2 configuration in figure 3 were closed during these tests.

Longitudinal controls used during these tests consisted of canard surfaces and a horizontal tail. The canard surfaces were attached to the sides of the body in the vicinity of the canopy with fixed dihedral of -20°. The horizontal tail was located below the wing-chord plane

and could be set at dihedral angles of 0° and -20°. The vertical tail was fixed at 0° incidence.

The body was representative of current high-speed fighter configurations having a high-fineness-ratio forebody and twin-engine nacelles designed as an integral part of the body. Horizontal ramp inlets having a capture area of 6.020 sq in. were utilized. The ratio of capture area to exit area was 0.847.

The model was mounted in the tunnel on a remotely controlled rotary sting. Forces and moments were measured by means of a six-component internal strain-gage balance.

TESTS, CORRECTIONS, AND ACCURACY

The test conditions are as follows:

Mach number	1.97
Stagnation temperature, $^\circ F$	100
Stagnation pressure, lb/sq ft	576
Reynolds number, based on $\bar{c}$ of W_2	1.503×10^6

The stagnation dewpoint was maintained sufficiently low (-25° or less) so that no condensation effects were encountered in the test section. Tests were made for an angle-of-attack range at $\beta = 0^\circ$ from approximately -4° to 8° and through a range of sideslip angles from approximately -4° to 6° at angles of attack of -0.5°, 4.0°, and 8.5°. The angle of attack and sideslip was corrected for deflection of the balance and sting under load. The pressure at the body base and within the balance enclosure was measured, and the drag force was adjusted to a base pressure equal to free-stream static pressure. The base drag coefficient was constant for the angle-of-attack range and amounted to 0.0028. The internal drag was determined from the change in momentum from free-stream conditions to measured conditions at the duct exit. The average mass-flow ratio through the inlet was 1.08. The internal drag coefficient was 0.0015 and the associated correction to normal-force coefficient was 0.00026 per degree of angle of attack.

Transition was fixed on all surfaces including the body. No. 80. carborundum grains were applied along the 10-percent-chord line of wing and tail surfaces. The body transition strip was applied at 10 percent of the body length rearward of the nose.

The estimated errors in the individual measured quantities based on a static calibration are as follows:

C_L	±0.0090
C_D	±0.0006
C_m	±0.0008
C_l	±0.0003
C_n	±0.0005
C_Y	±0.0037
α, deg	±0.1
β, deg	±0.1
M	±0.01

PRESENTATION OF RESULTS

The longitudinal and lateral aerodynamic characteristics of model configurations equipped with wings 1 and 3 are presented in figures 4 to 15. The aerodynamic characteristics of the model configurations equipped with wing 2 are presented in figures 16 to 20. A comparison of the longitudinal aerodynamic characteristics of the model with wings 1 and 2 is shown by results presented in figure 21. In many of these figures the drag results have been omitted because of a strain-gage malfunction. An index of figures is presented in table II.

DISCUSSION

Longitudinal Stability

An investigation of the present airplane configuration utilizing wings 1 and 2 at subsonic speeds (ref. 7) indicated that the change in longitudinal stability with wing sweep angle was appreciably smaller with wing 1 than with wing 2. A comparison of the longitudinal stability characteristics at supersonic speeds of this configuration with wing 1 ($\Lambda = 75^\circ$) and wing 2 ($\Lambda = 70.5^\circ$) is presented in figure 21. In general, the variation of pitching moment with lift coefficient for both wings 1 and 2 was linear. The static margin with wing 1 was 23 percent $\bar{c}$; whereas with wing 2 it was 21 percent $\bar{c}$. Although lack of data for the configuration with wing 2 precludes a comparison of drag of the two wing configurations, results presented in figure 10 indicate that the minimum drag coefficient of the configuration with the body, wing 1, and tails was 0.025 and the untrimmed $(L/D)_{max}$ was 5.0. The use of canard surfaces as a destabilizing device resulted in a decrease

in static margin of approximately 8 percent $\bar{c}$ which resulted in a static margin of 15 percent $\bar{c}$ for the configuration with wing 1 and a horizontal-tail dihedral of -20° (fig. 11). Removal of the horizontal tail decreased the static margin to 2 percent $\bar{c}$. From these results and results of reference 7 it is of interest to note that the total change in static margin due to an increase in wing sweep angle from 25° to 75° combined with an increase in Mach number from 0.25 to 1.97 amounts to about 18 percent $\bar{c}$ for the configuration with the body, wing 1 (outboard pivot), and horizontal tail. However, for the configuration with wing 2 (inboard pivot), the corresponding shift is 26 percent $\bar{c}$ for 10° less variation in sweep (30° to 70.5°). This substantiates the advantage of the pivot location of wing 1 anticipated in reference 7.

The effect of an increase in the sweep angle from 75° to 113° is of interest from the point of view of low-altitude flight. The results obtained with wing 3 (actually wing 1 with leading edge swept back 113°) are presented in figure 12. Increasing the wing sweep angle from 75° to 113° resulted in a decrease in lift-curve slope of approximately 22 percent and a decrease in static margin of 9 percent $\bar{c}$ while the effectiveness of the horizontal tail (Γ = -20°) increased from 0.0055 to 0.0060. In addition, the minimum drag for the 75° and 113° wing configuration was essentially the same; however, the untrimmed $(L/D)_{max}$ decreased from 5.0 to approximately 4.5 with increase in wing sweep. (See figs. 10 and 12.)

Lateral Stability

The various configurations tested at M = 1.97 indicate that the lateral and directional stability characteristics were not appreciably different from the characteristics at subsonic speeds (ref. 7). The configuration with wing 1 and tails (Γ = 0° or -20°) indicates positive directional stability and positive effective dihedral $\left(-C_{l_\beta}\right)$ throughout the angle-of-attack range. (See fig. 15.) The effects of horizontal-tail dihedral (fig. 15) are similar to the dihedral effects indicated in reference 5. The lateral and directional characteristics for the configuration with wing 2 were similar to those for the configuration with wing 1. The decrease in directional stability with angle of attack for the wing-tail configurations results from a loss in vertical-tail contribution as well as an increase in instability of the wing-body configuration. The addition of canards has an adverse effect on C_{n_β} (fig. 20). This adverse effect of canard surfaces as evidenced by an increase in instability of the vertical-tail-off configuration (fig. 19) is due to the negative geometric dihedral of the canard surfaces.

CONCLUDING REMARKS

An investigation has been conducted in the Langley 4- by 4-foot supersonic pressure tunnel at a Mach number of 1.97 to determine the stability and control characteristics of a fighter-type aircraft configuration having two types of variable-sweep wings. One wing had an outboard pivot and the other an inboard pivot.

The results for the configuration with wing, body, and tails exhibited a linear variation of pitching moment with lift coefficient, positive directional stability, and positive effective dihedral with either wing 1 or 2.

These results, in conjunction with low-speed results for the same model obtained from NASA Technical Memorandum X-303, indicate that the total change in static margin due to increasing the Mach number and changing the wing sweep from 25° to 75° is about 18 percent of the mean geometric chord for the outboard-pivot configuration and about 26 percent of the mean geometric chord for the inboard-pivot configuration for a sweep-angle variation from 30° to 70.5°.

Langley Research Center,
National Aeronautics and Space Administration,
Langley Field, Va., June 8, 1960.

REFERENCES

1. Alford, William J., Jr., and Henderson, William P.: An Exploratory Investigation of the Low-Speed Aerodynamic Characteristics of Variable-Wing-Sweep Airplane Configurations. NASA TM X-142, 1959.

2. Alford, William J., Jr., Lucma, Arvo A., and Henderson, William P.: Wind-Tunnel Studies at Subsonic and Transonic Speeds of a Multiple-Mission Variable-Wing-Sweep Airplane Configuration. NASA TM X-206, 1959.

3. Spearman, M. Leroy, and Foster, Gerald V.: Stability and Control Characteristics at a Mach Number of 2.01 of a Variable-Wing-Sweep Configuration With Outboard Wing Panels Swept Back 75°. NASA TM X-32, 1959.

4. Foster, Gerald V.: Stability and Control Characteristics at Mach Numbers of 2.50, 3.00, and 3.71 of a Variable-Wing-Sweep Configuration With Outboard Wing Panels Swept Back 75°. NASA TM X-267, 1960.

5. Spearman, M. Leroy, and Foster, Gerald V.: Effects of Various Modifications on the Supersonic Stability Characteristics of a Variable-Wing-Sweep Configuration at a Mach Number of 2.01. NASA TM X-260, 1960.

6. Foster, Gerald V.: Effects of Spoiler-Slot-Deflector Control on the Aerodynamic Characteristics at a Mach Number of 2.01 of a Variable-Wing-Sweep Configuration With the Outer Wing Panels Swept Back 75°. NASA TM X-273, 1960.

7. Spencer, Bernard, Jr.: Stability and Control Characteristics at Low Subsonic Speeds of an Airplane Configuration Having Two Types of Variable-Sweep Wings. NASA TM X-303, 1960.

8. Bielat, Ralph P., Robins, A. Warner, and Alford, William J., Jr.: The Transonic Aerodynamic Characteristics of Two Variable-Sweep Airplane Configurations Capable of Low-Level Supersonic Attack. NASA TM X-304, 1960.

TABLE I.- GEOMETRIC CHARACTERISTICS OF MODEL

Wing 1:	
Area, including body intercept, sq ft	3.35
Span, in.	30.20
Mean geometric chord, in.	18.21
Aspect ratio	1.89
Sweep of leading edge (sections outboard of pivot), deg	75
Dihedral, deg	0
Twist, deg	0
Incidence, deg	0
Airfoil section of outboard panel (measured streamwise when wing swept 25.00°)	NACA 65A006
Airfoil section of inboard panel (measured streamwise)	NACA 65A004.5
Root chord, in.	25.87
Tip chord, in.	2.32
Wing 2:	
Area, sq ft	3.33
Span, in.	28.99
Mean geometric chord, in.	19.13
Aspect ratio	1.75
Taper ratio	0.11
Sweep of leading edge (sections outboard of pivot), deg	70.50
Dihedral, deg	0
Twist, deg	0
Incidence, deg	0
Airfoil section of outboard panel (measured streamwise when wing is swept 43.05°)	NACA 65A005
Root chord, in.	32.35
Tip chord, in.	3.45
Horizontal tail ($\Gamma = 0°$):	
Area (exposed), sq ft	0.96
Span, in.	26.60
Taper ratio	0.20
Sweepback of quarter-chord line, deg	45
Poot chord (exposed), in.	11.71
Tip chord, in.	2.30
Vertical tail:	
Area (exposed), sq ft	0.48
Span (above fuselage center line), in.	12.13
Taper ratio	0.35
Sweep of quarter-chord line, deg	45.00
Tip chord, in.	3.51
Root chord (exposed), in.	10.03
Canard control:	
Area, sq ft	0.26
Semispan (measured in plane of canard surface), in.	4.71
Taper ratio	0.40
Sweep of leading edge, deg	43
Sweep of trailing edge, deg	15
Airfoil section	Wedge
Root chord (fuselage center line), in.	5.67
Tip chord, in.	2.28
Dihedral, deg	-20

TABLE II.- INDEX OF FIGURES

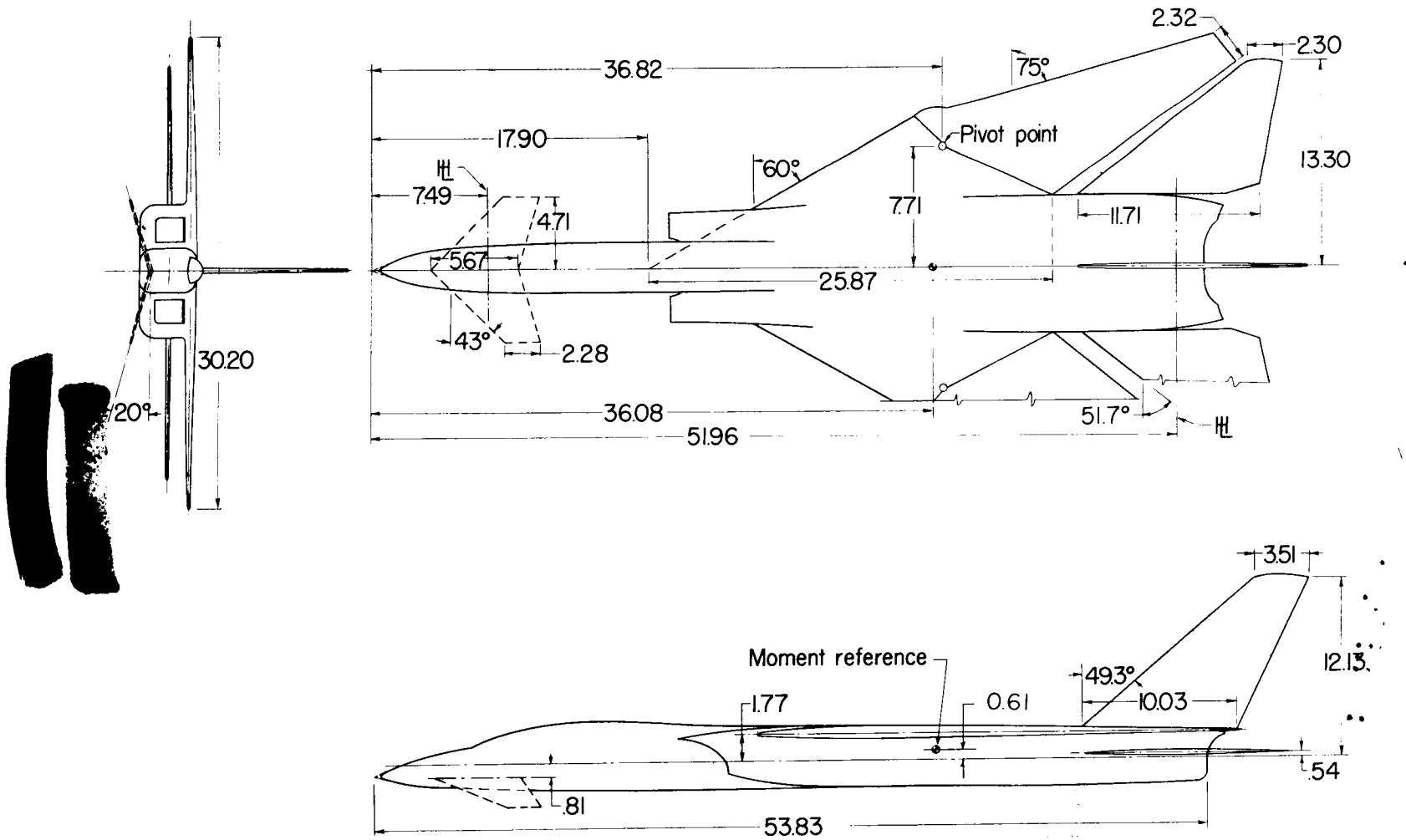

(a) Wing configuration 1 (outboard pivot).

Figure 1.- Details of models. All dimensions are in inches unless otherwise noted.

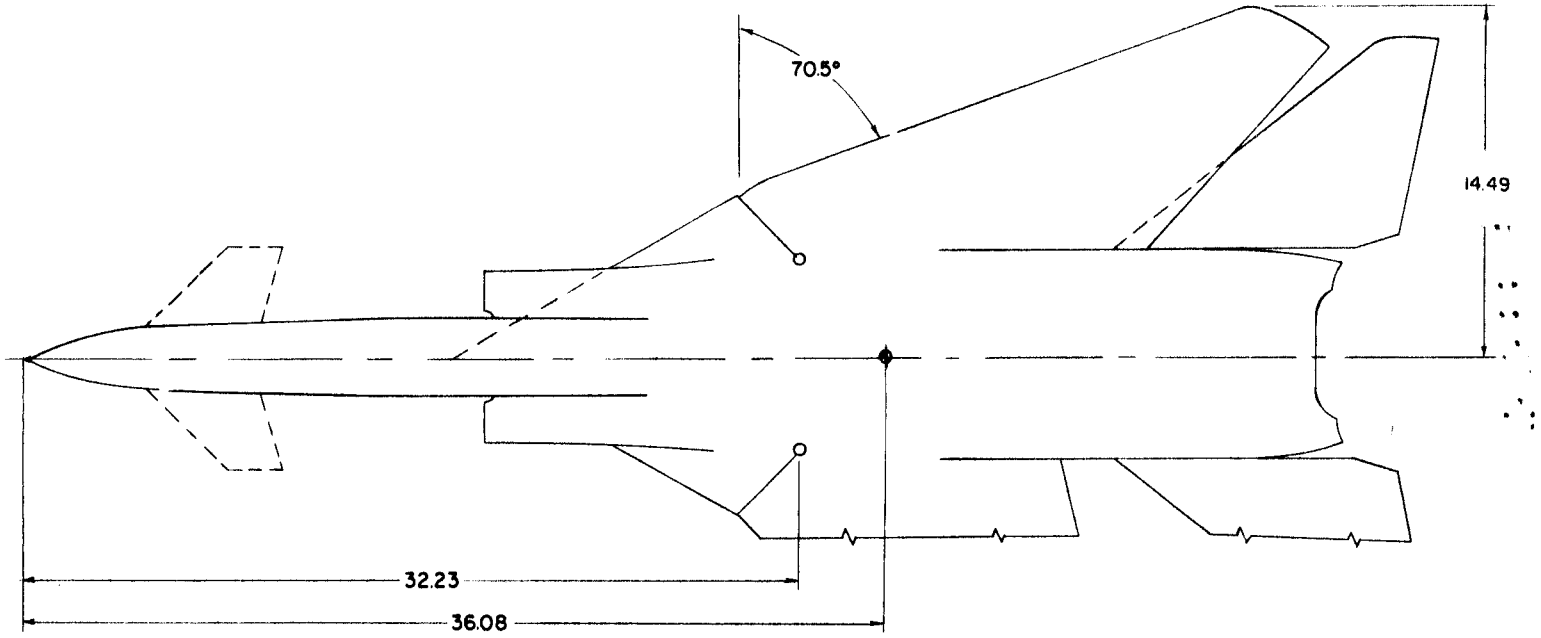

(b) Wing configuration 2 (inboard pivot).

Figure 1.- Continued.

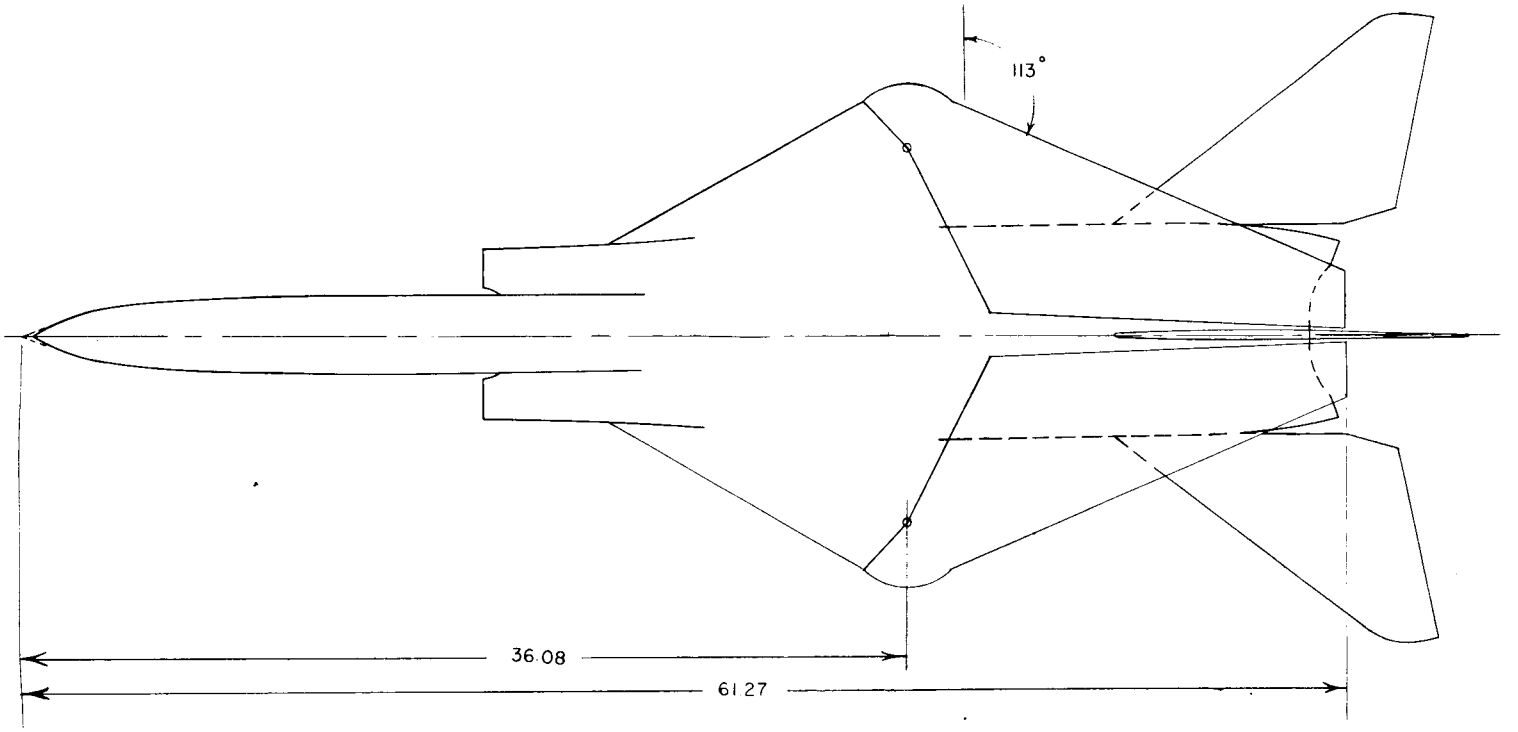

(c) Wing configuration 3.

Figure 1.- Concluded.

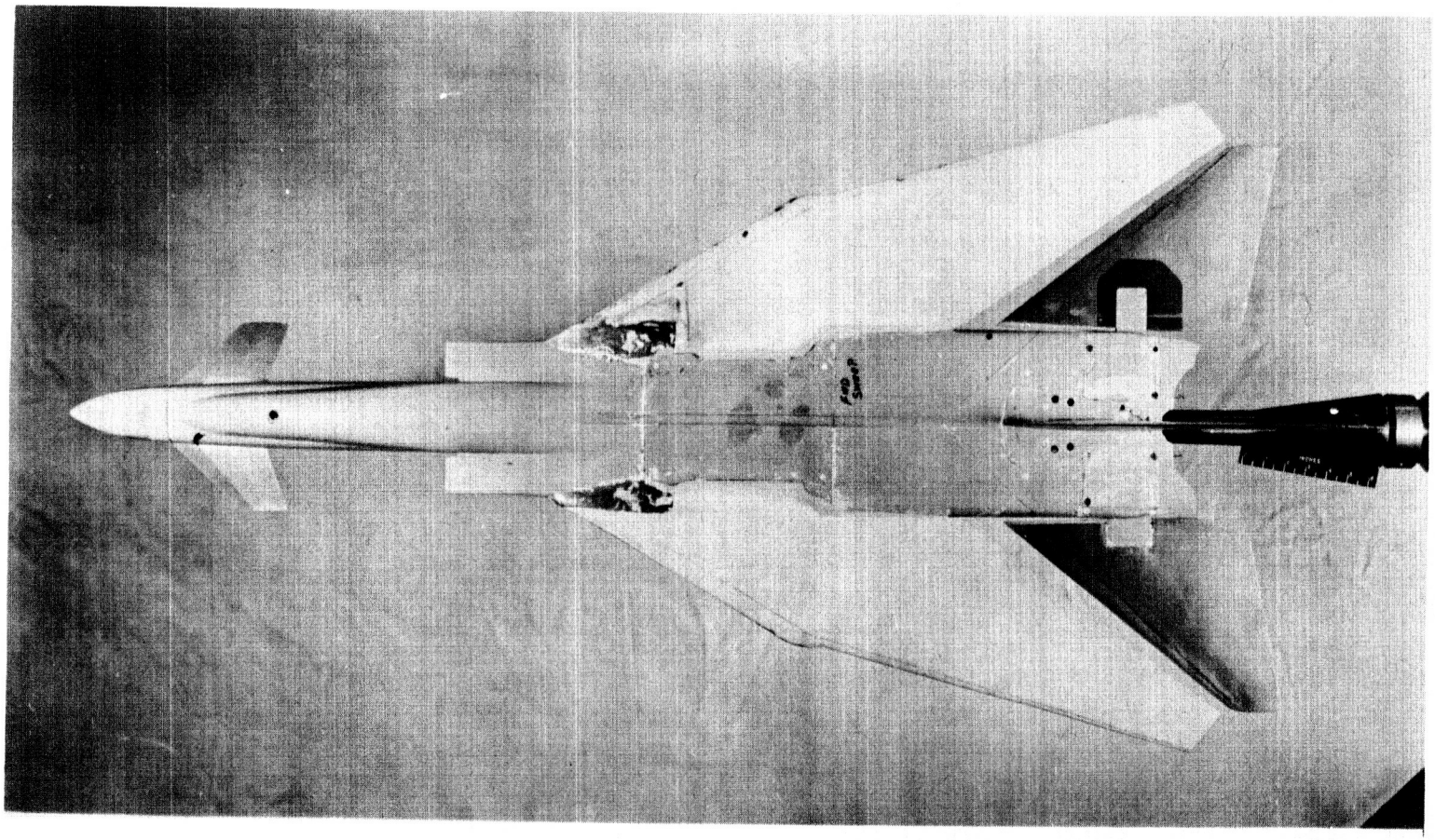

(a) Top view. L-60-447

Figure 2.- Photographs of model with wing configuration 1.

(b) Side view. L-60-450

Figure 2.- Concluded.

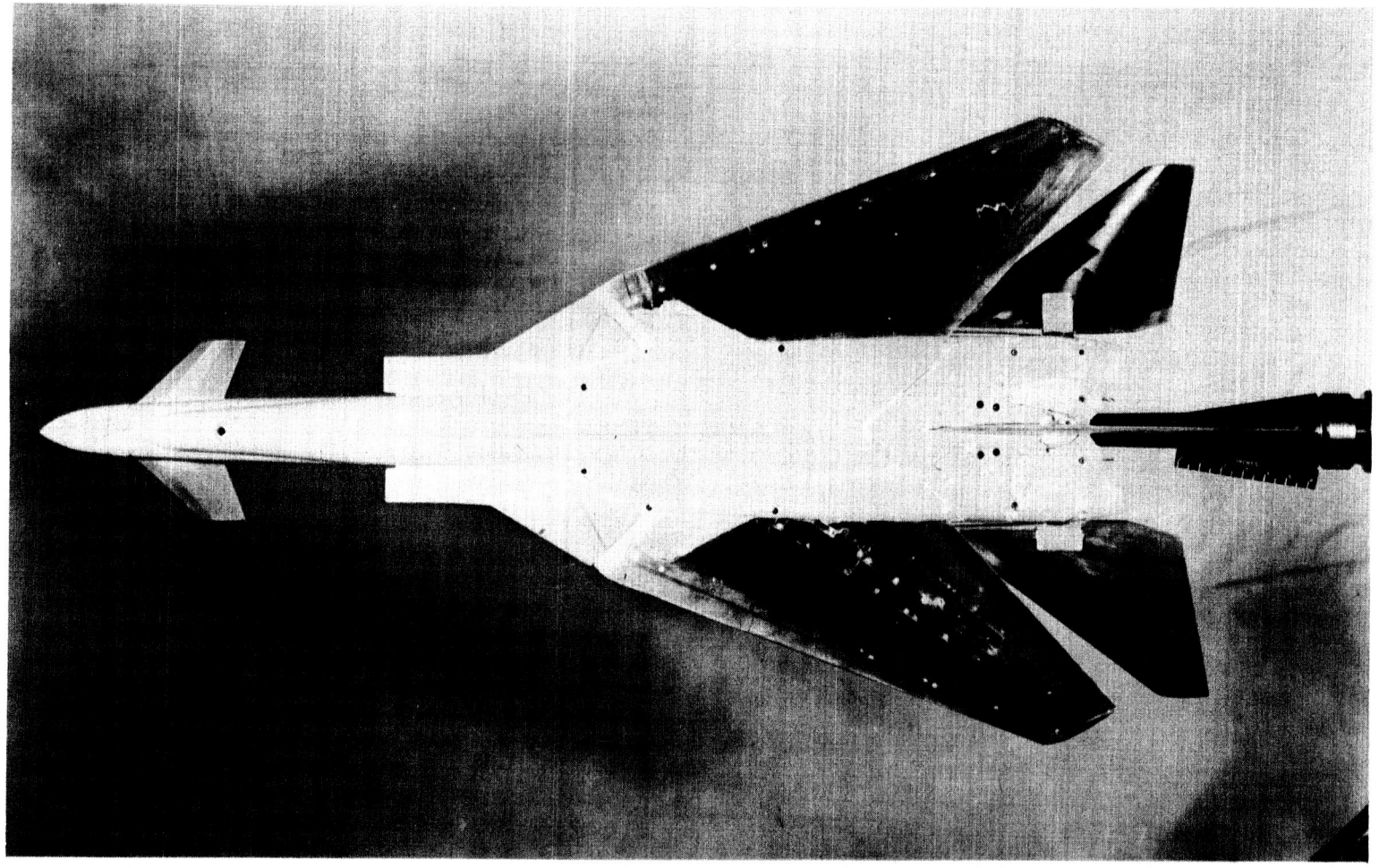

(a) Top view. L-60-448

Figure 3.- Photographs of model with wing configuration 2.

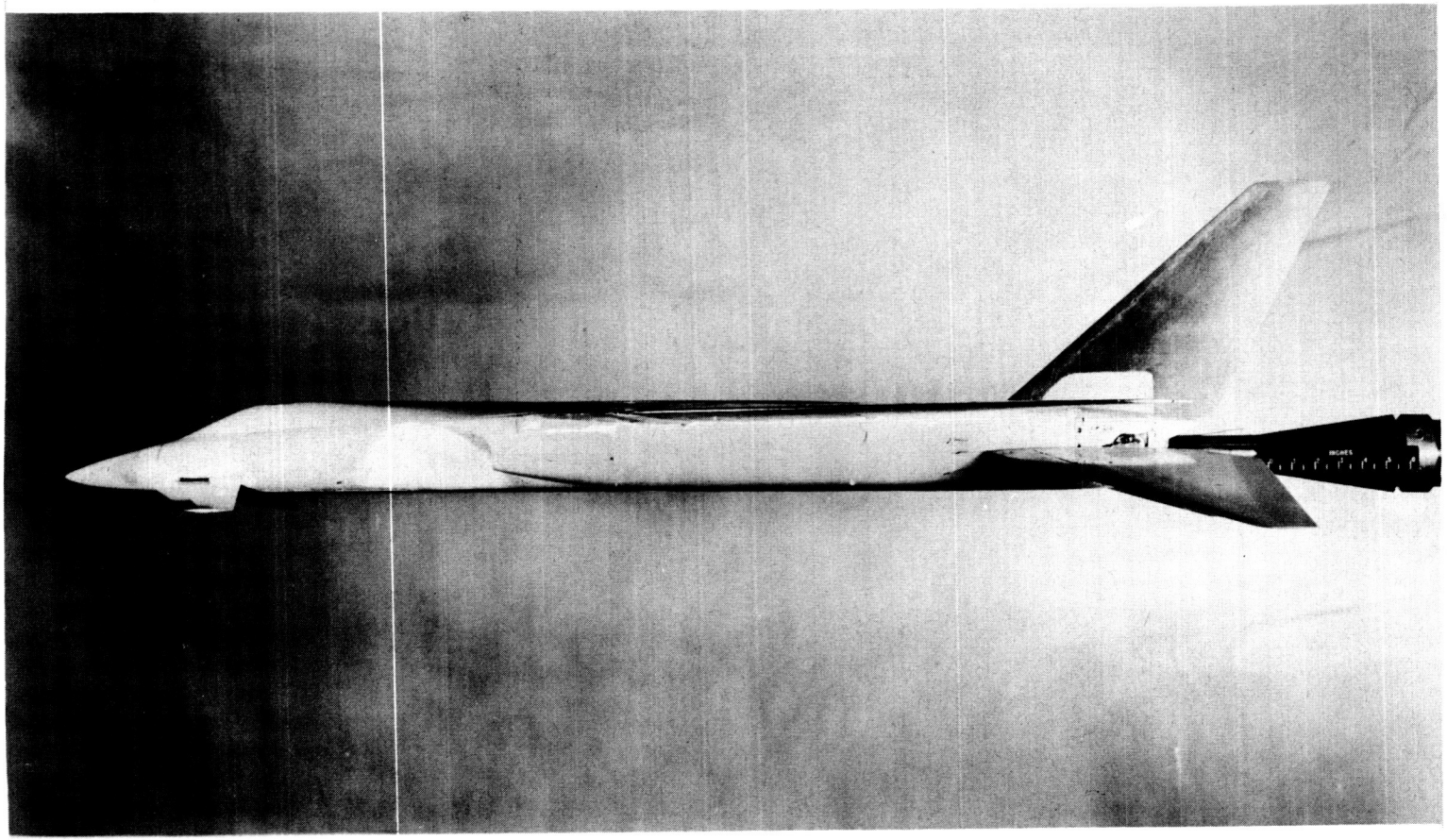

(b) Side view. L-60-451

Figure 3.- Continued.

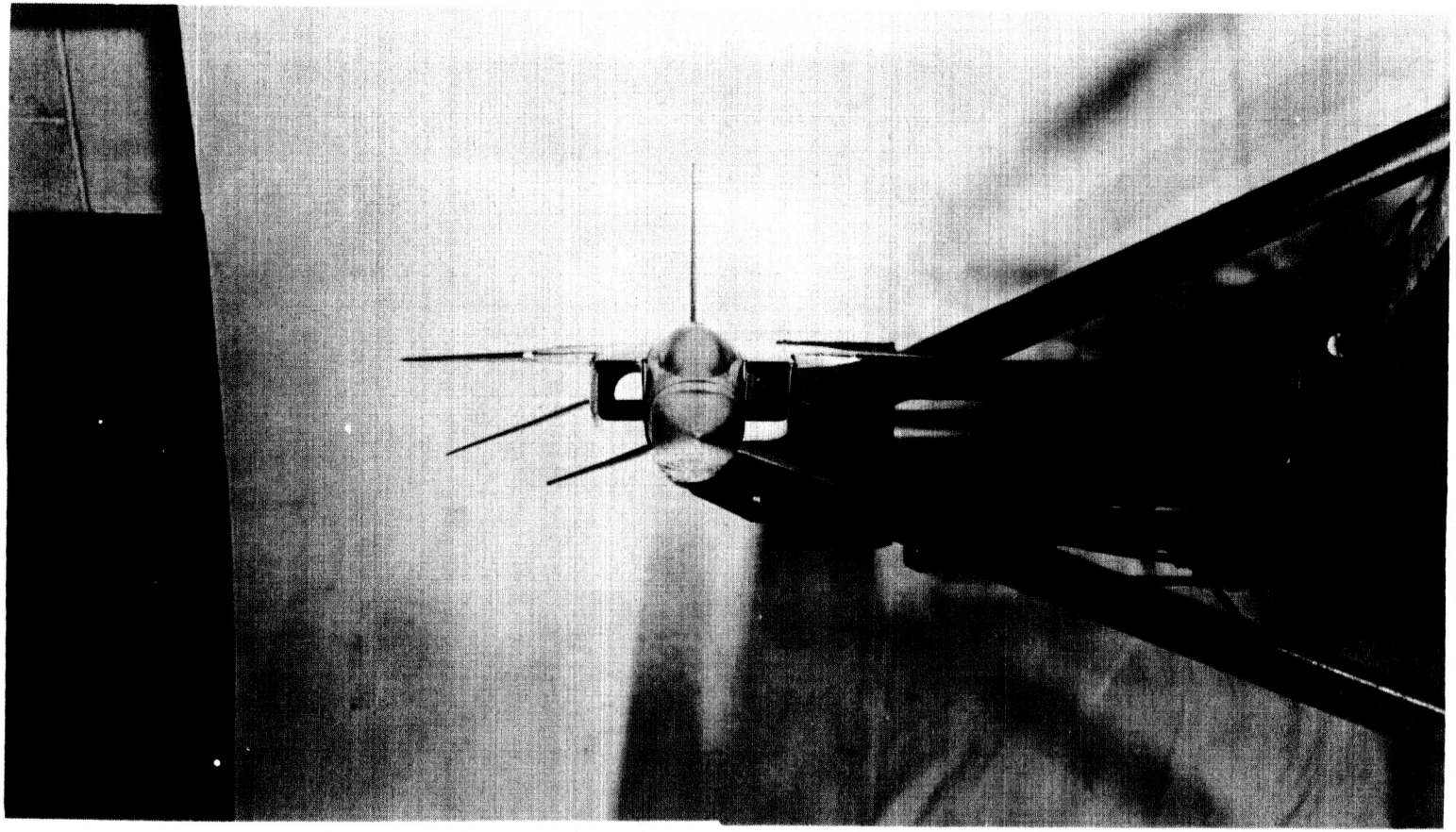

(c) Front view. L-60-449

Figure 3.- Concluded.

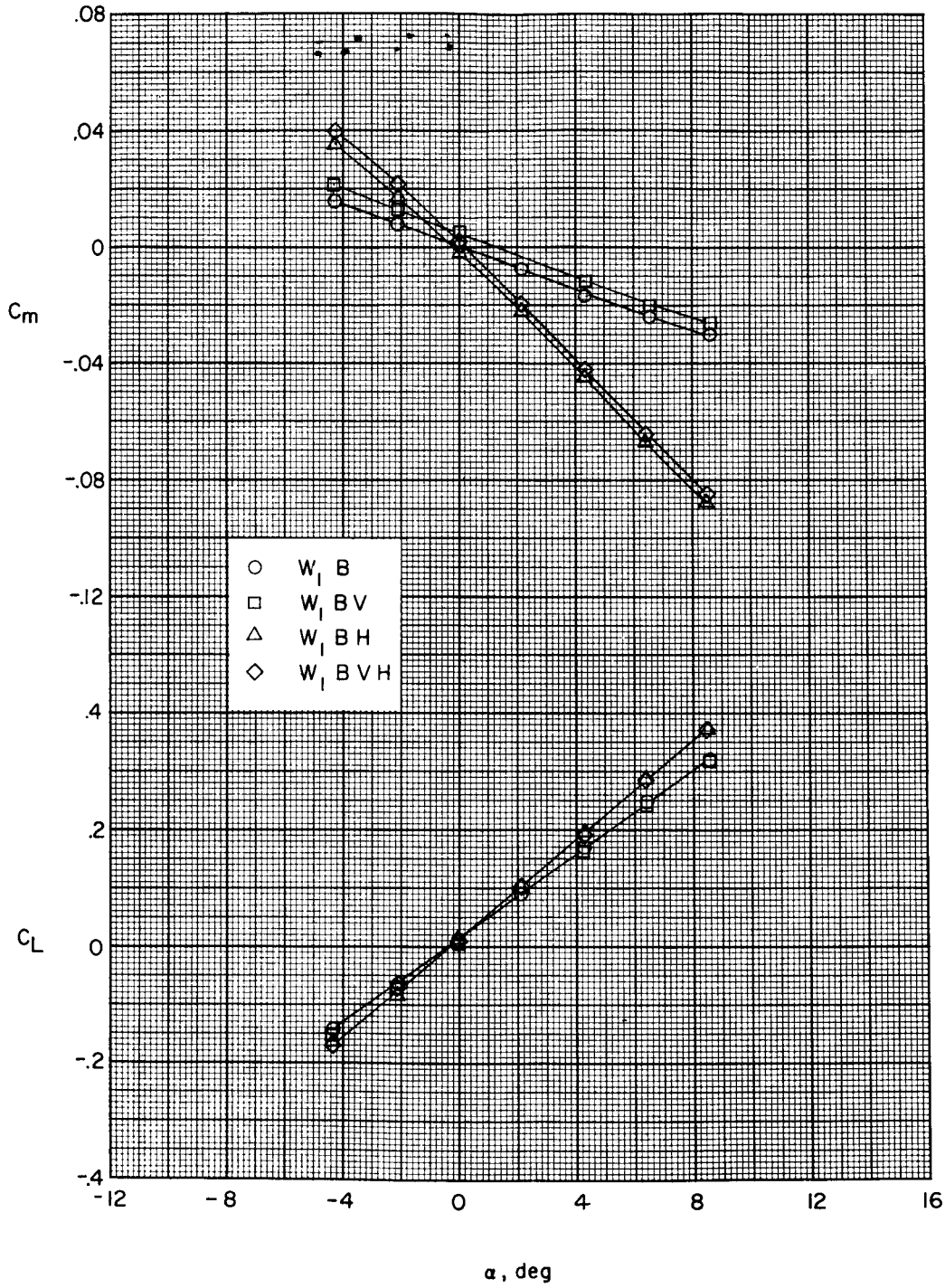

Figure 4.- Aerodynamic characteristics in pitch for various combination of components; wing 1; canard surface off; $\Gamma = 0^{\circ}$; $\delta_h = 0^{\circ}$.

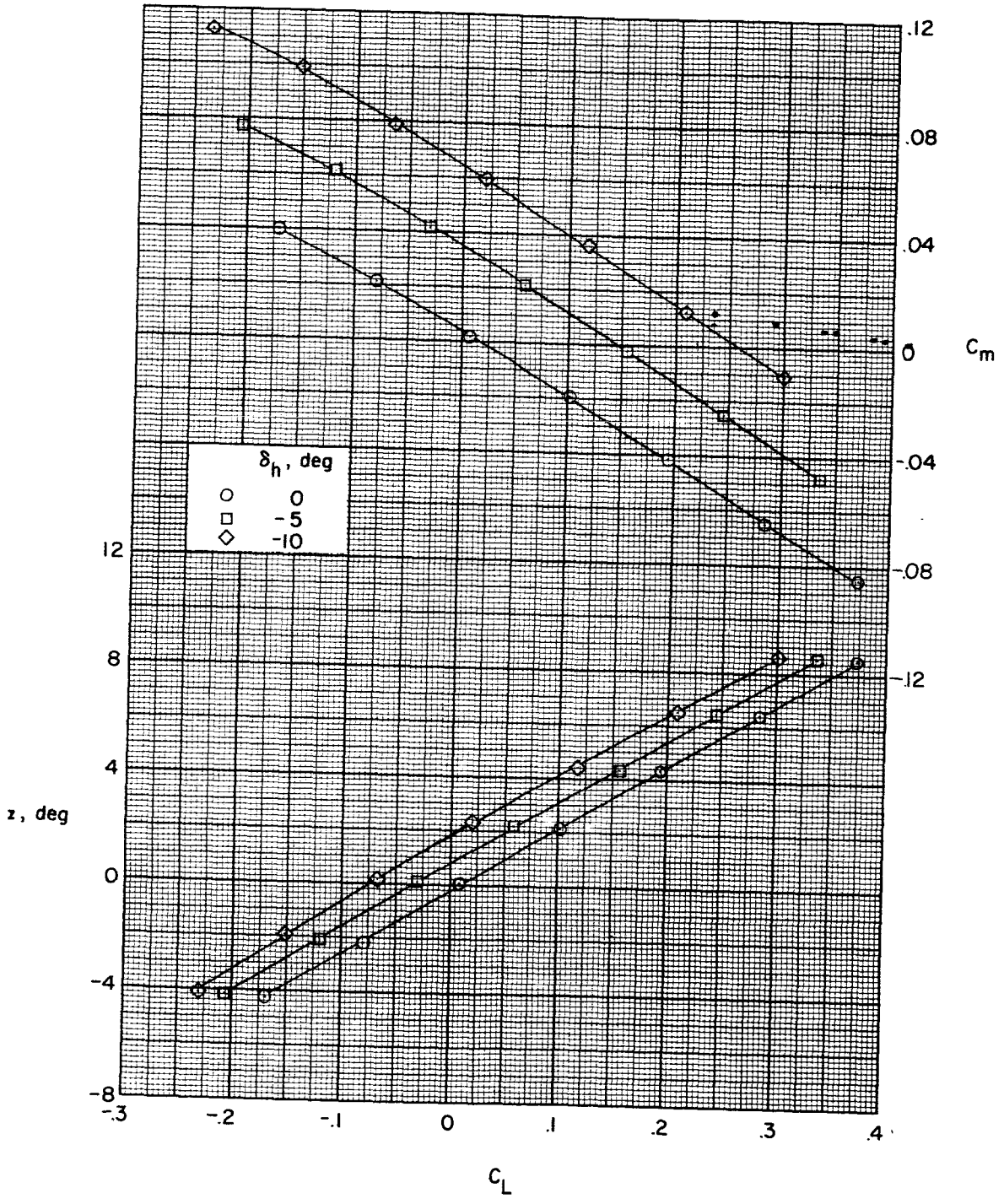

Figure 5.- Effect of horizontal-tail deflection on the aerodynamic characteristics in pitch; W_1BHV; canard surface off; $\Gamma = 0^\circ$.

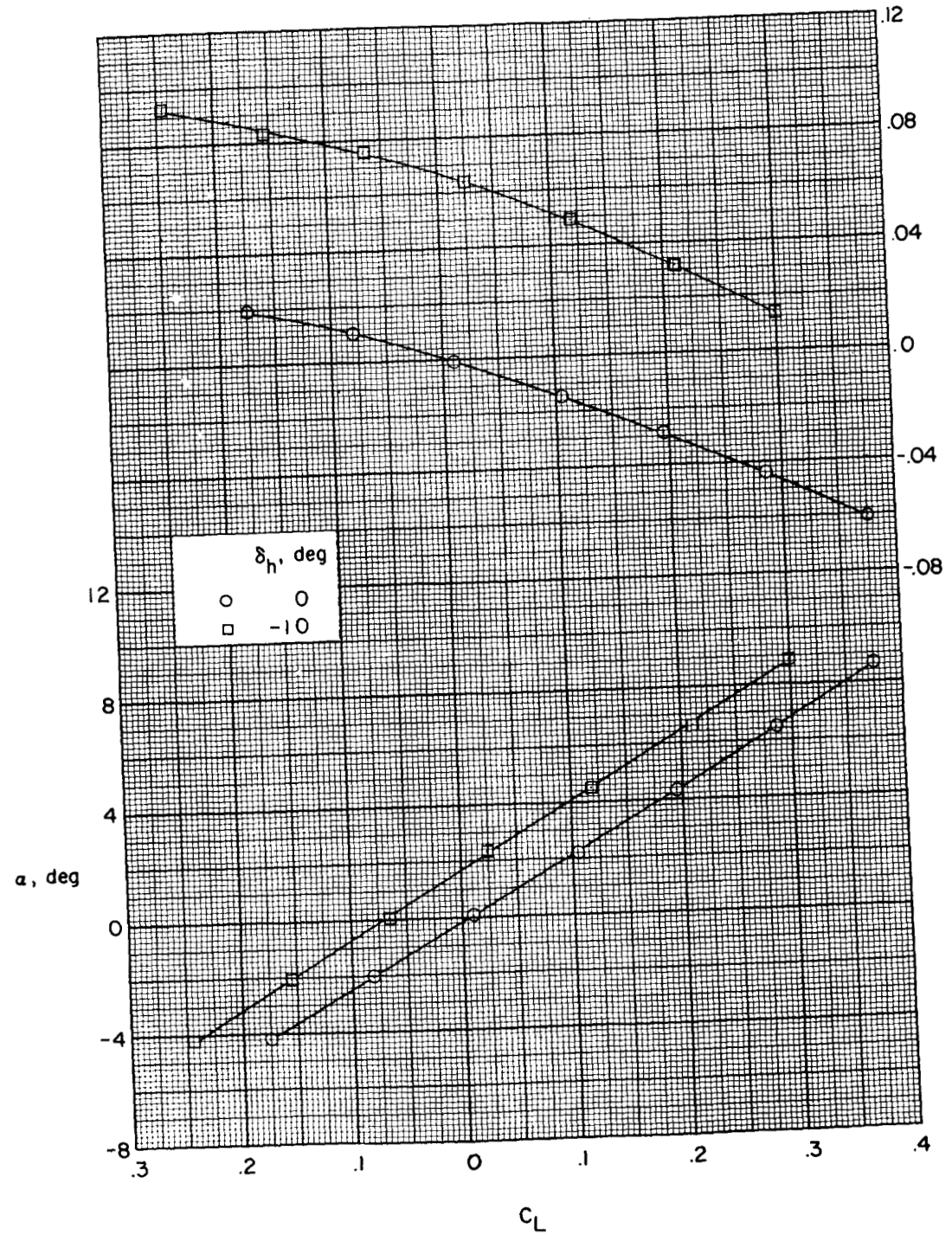

Figure 6.- Effect of horizontal-tail deflection on the aerodynamic characteristics in pitch; W_1BHVC; $\Gamma = 0^\circ$; $\delta_c = 0^\circ$.

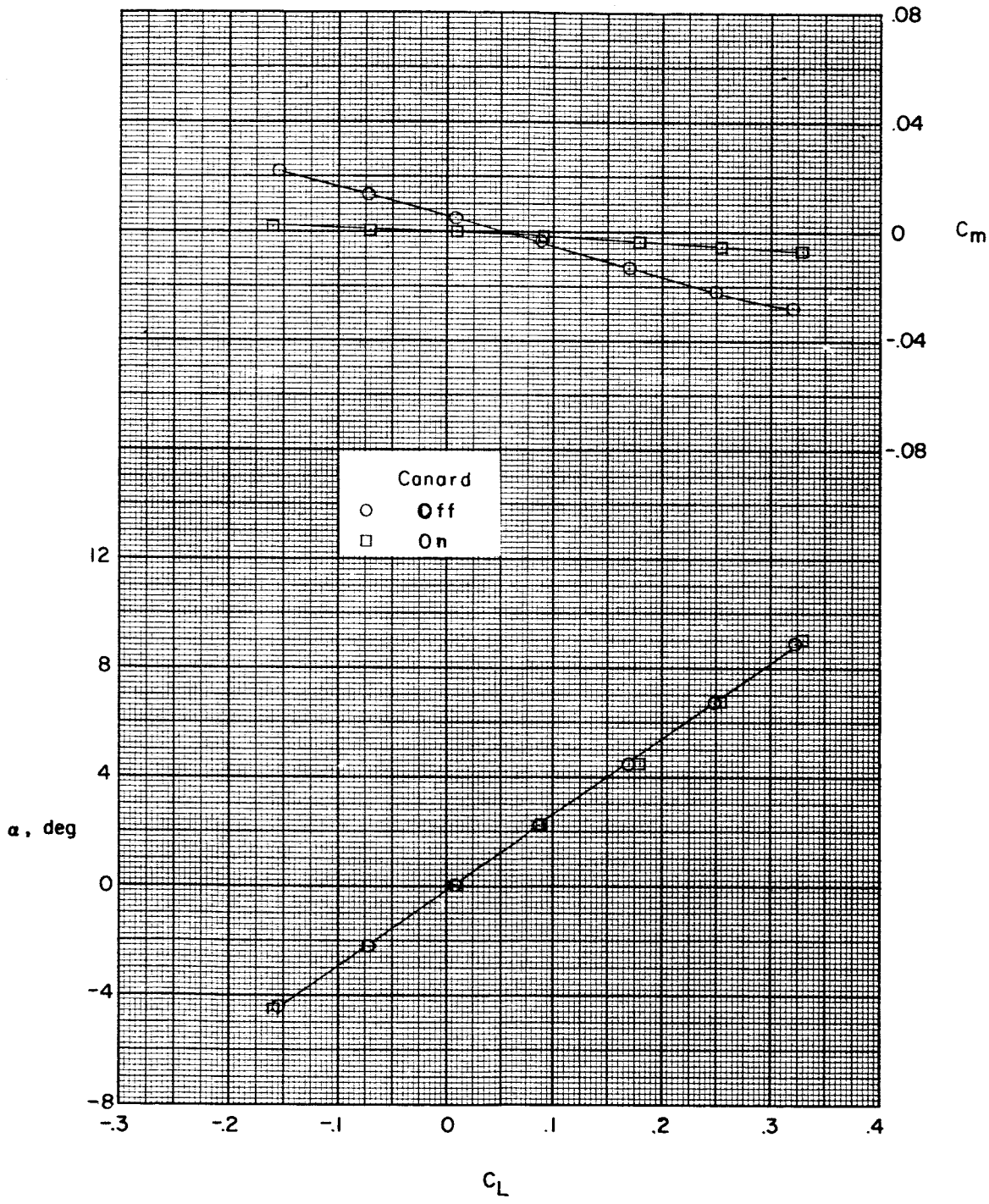

Figure 7.- Effect of canard surface on the aerodynamic characteristics in pitch; W_1BV.

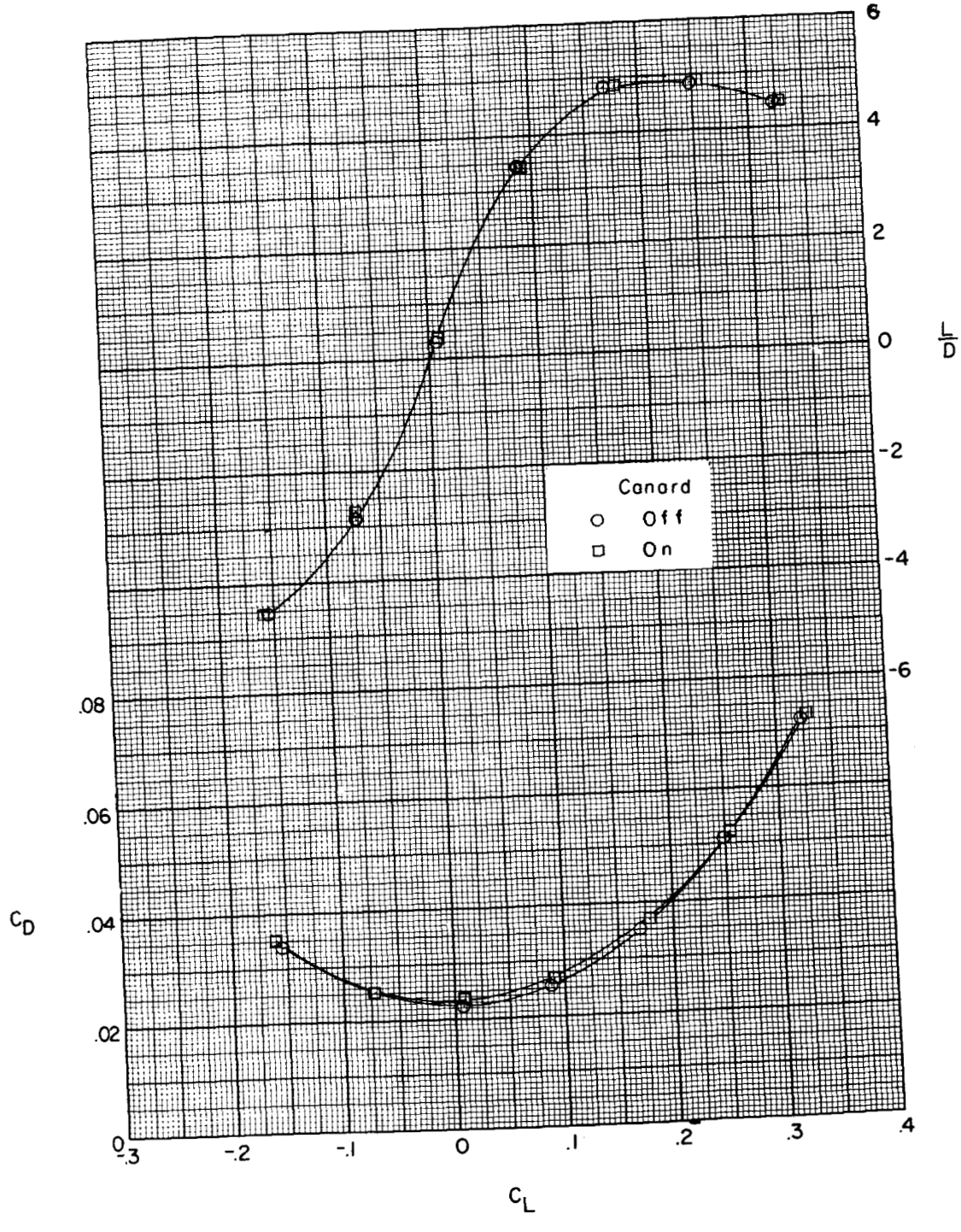

Figure 7.- Concluded.

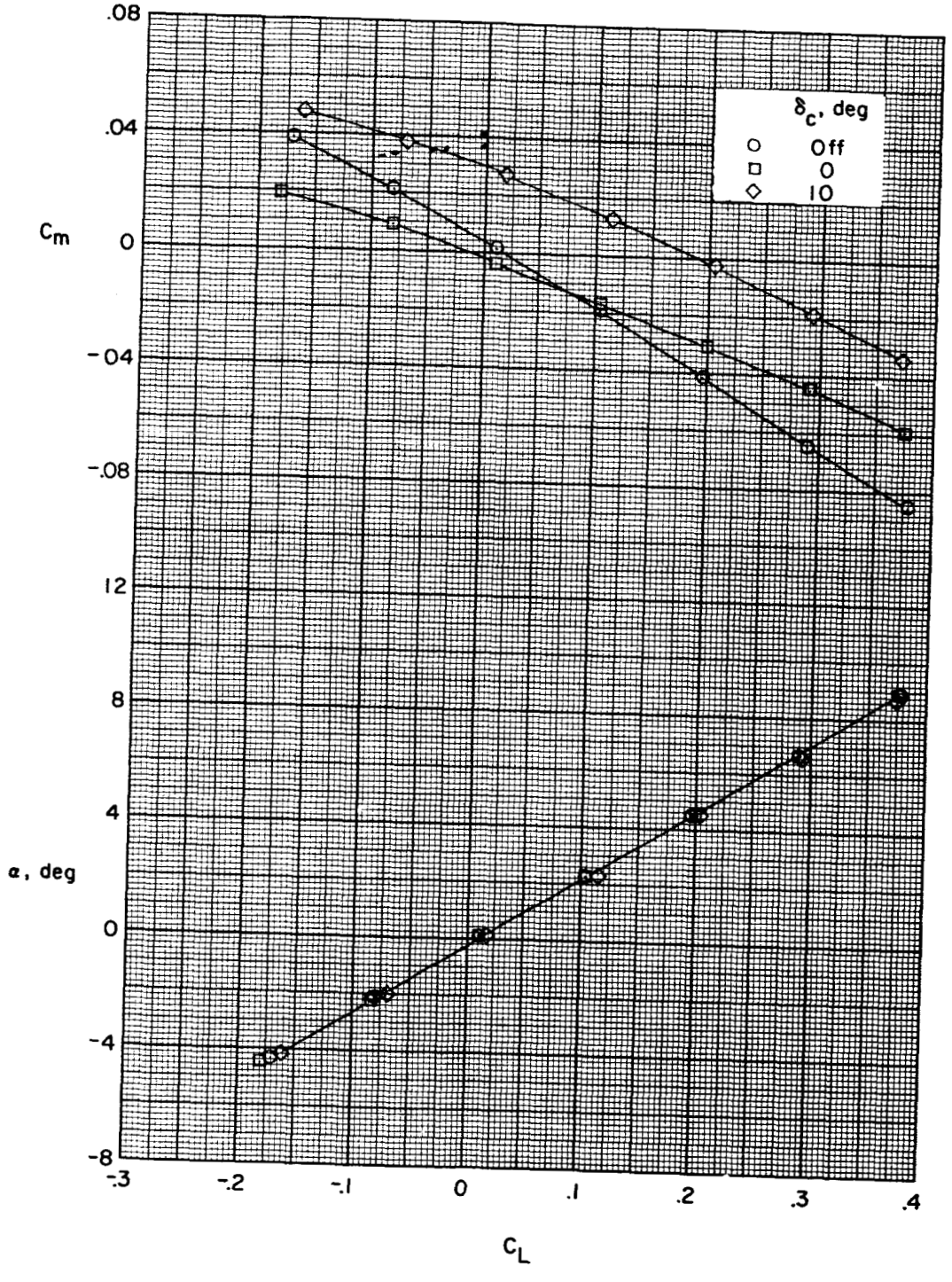

Figure 8.- Effect of canard surface on the longitudinal aerodynamic characteristics in pitch; W_1BHV; $\Gamma = 0^o$; $\delta_h = 0^o$.

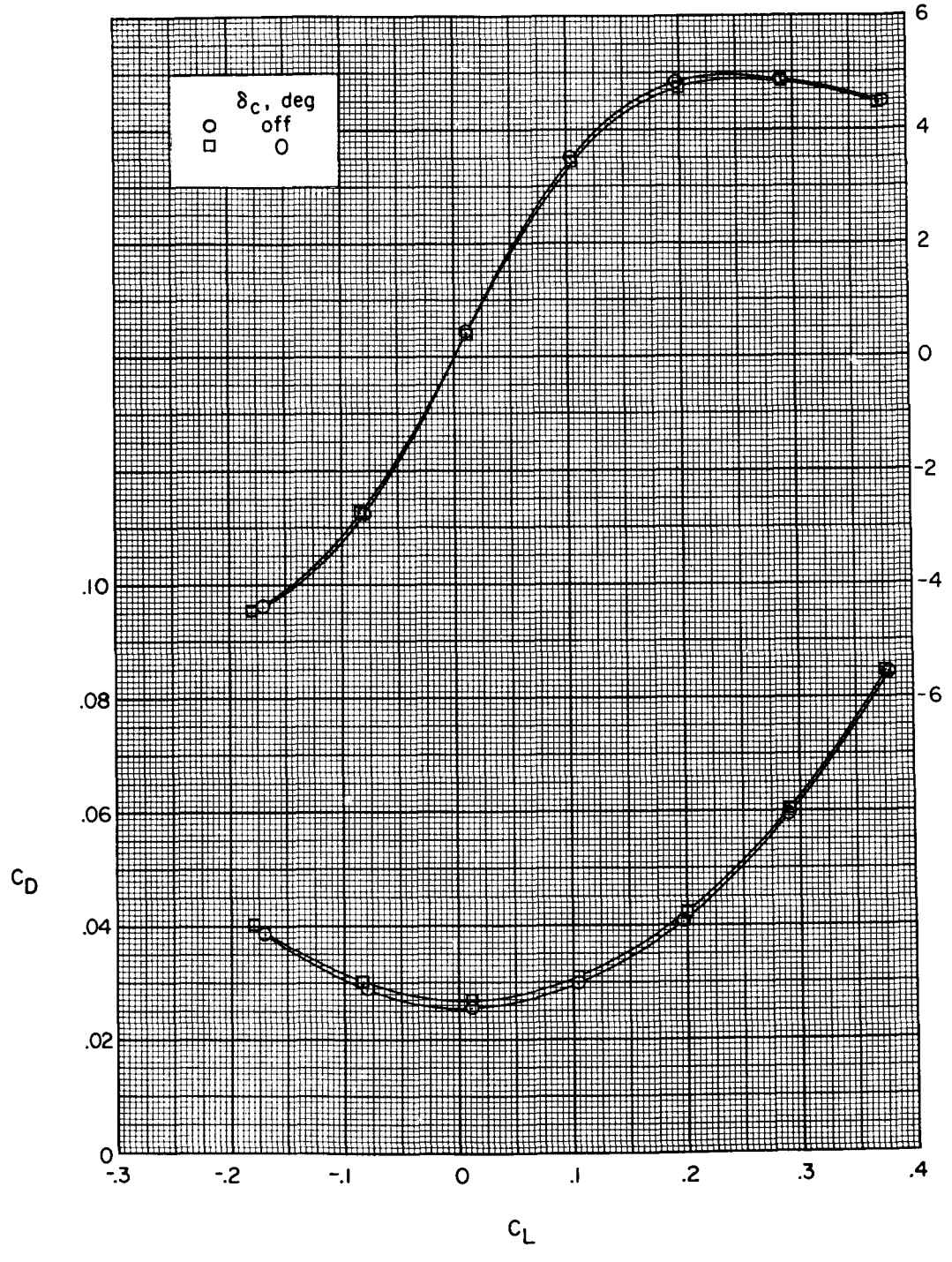

Figure 8.- Concluded.

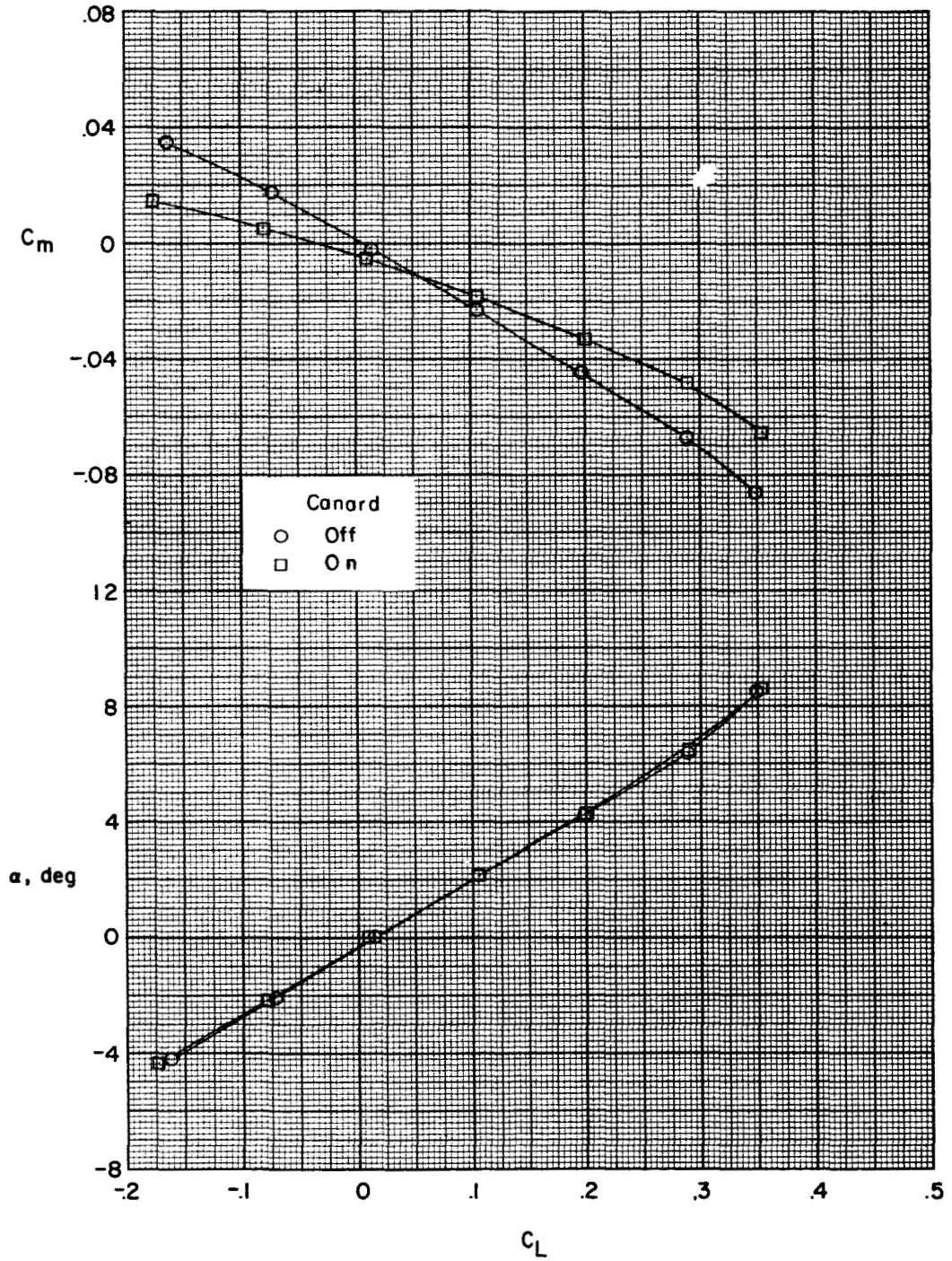

Figure 9.- Effect of canard surface on the aerodynamic characteristics in pitch; W_1BH; $\Gamma = 0^o$; $\delta_h = 0^o$.

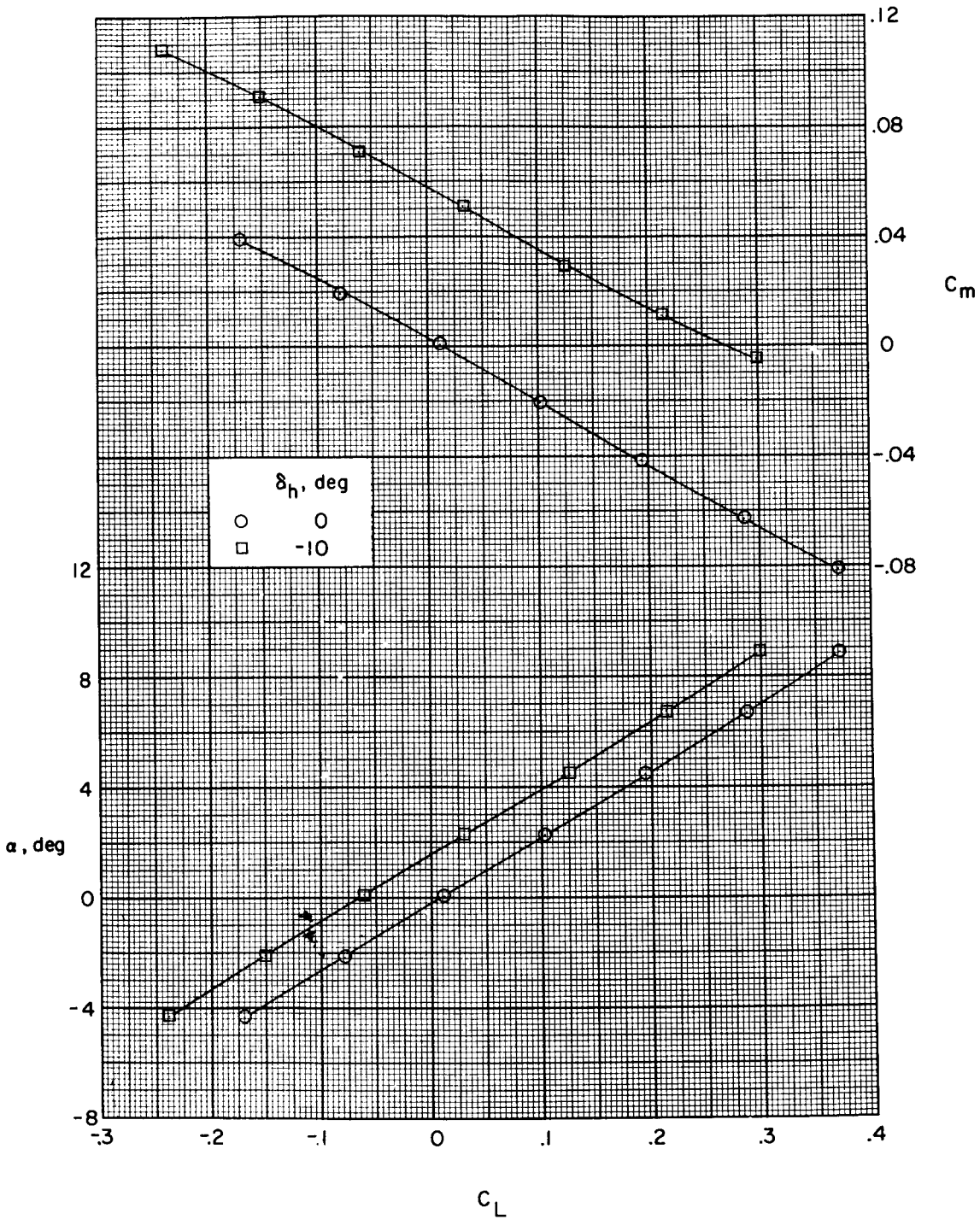

Figure 10.- Effect of horizontal-tail deflection on the aerodynamic characteristics in pitch; canard surface off; W_1BHV; $\Gamma = -20^\circ$.

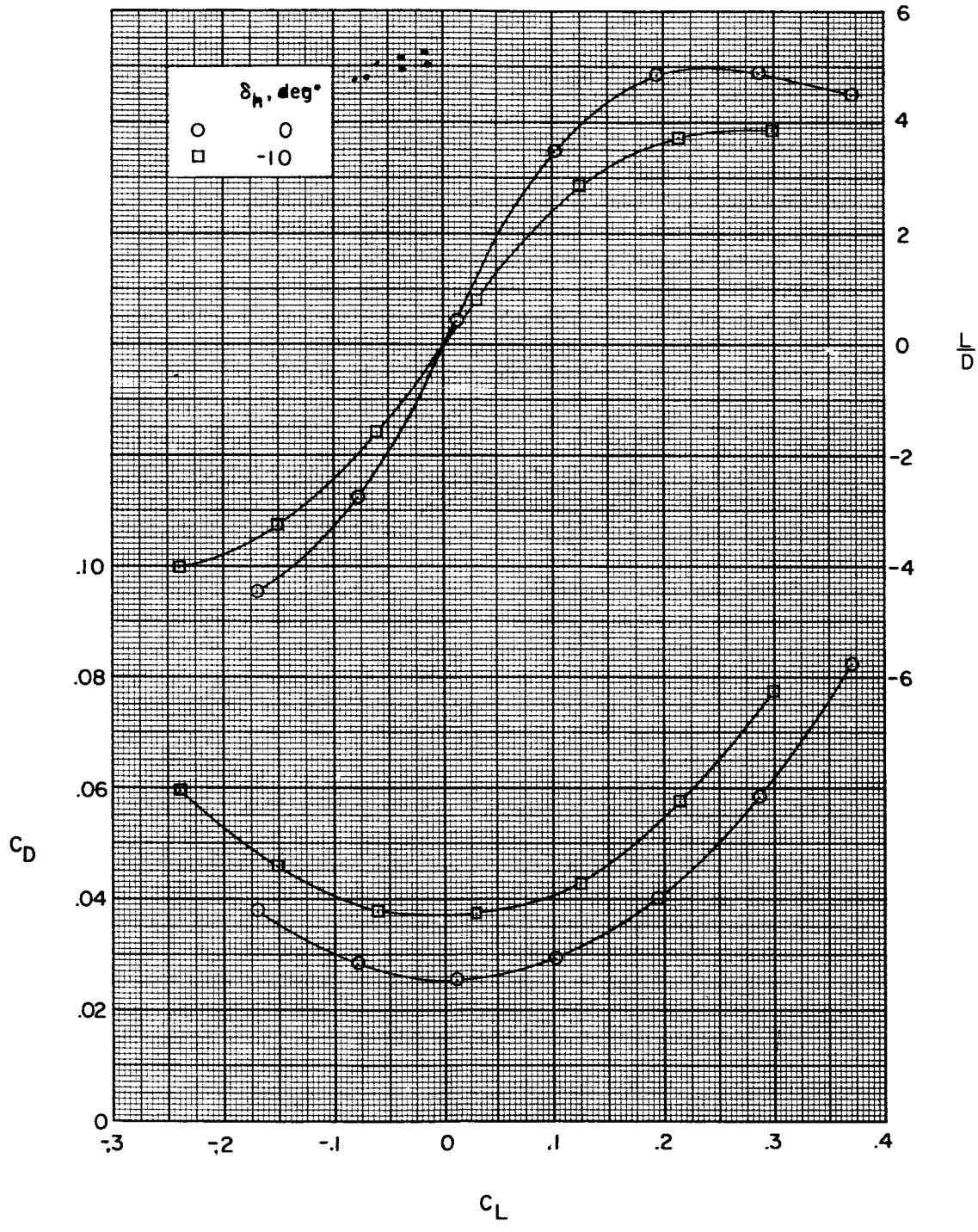

Figure 10.- Concluded.

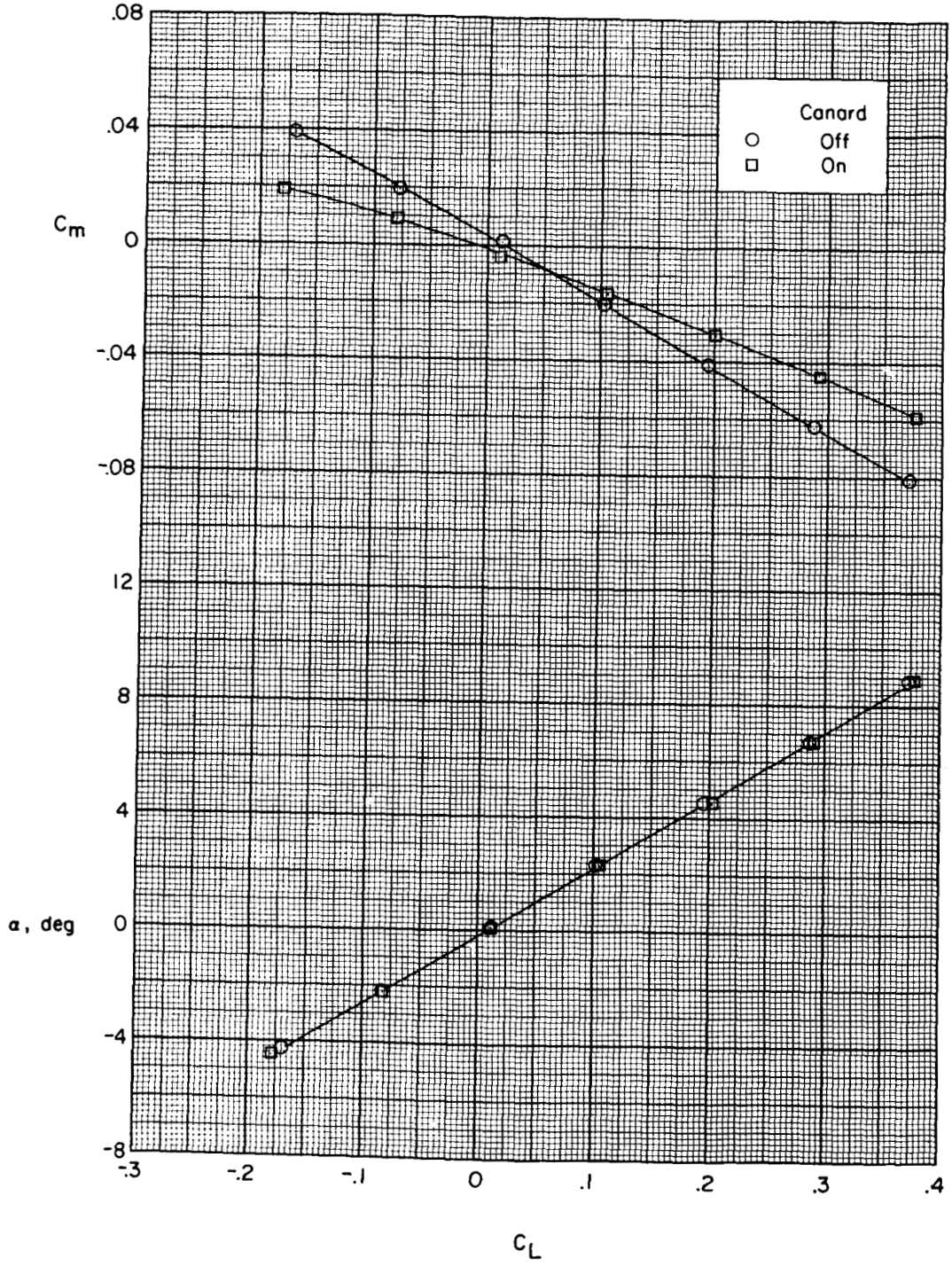

Figure 11.- Effect of canard surface on the longitudinal aerodynamic characteristics in pitch; W_1BHV; $\Gamma = -20^o$.

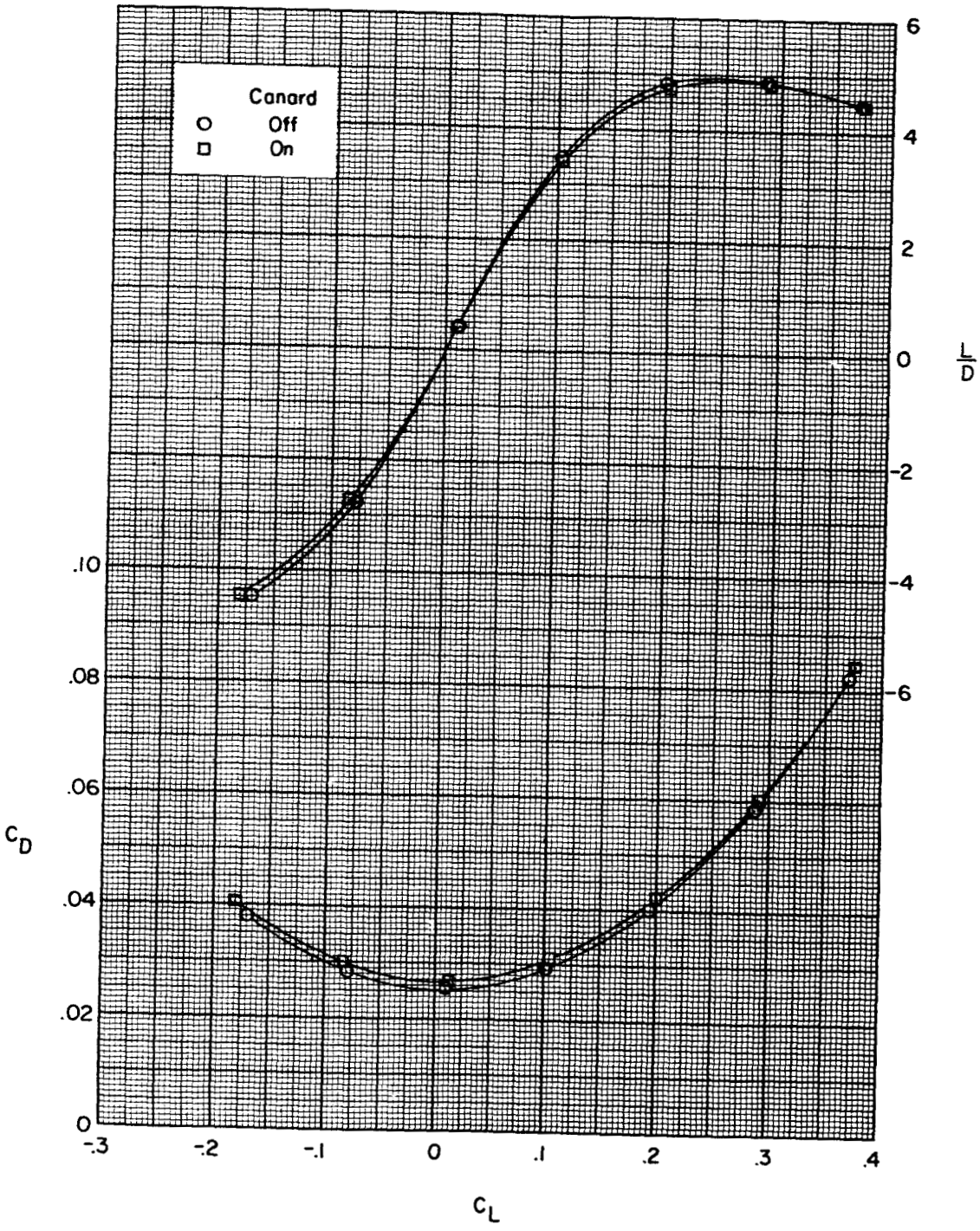

Figure 11.- Concluded.

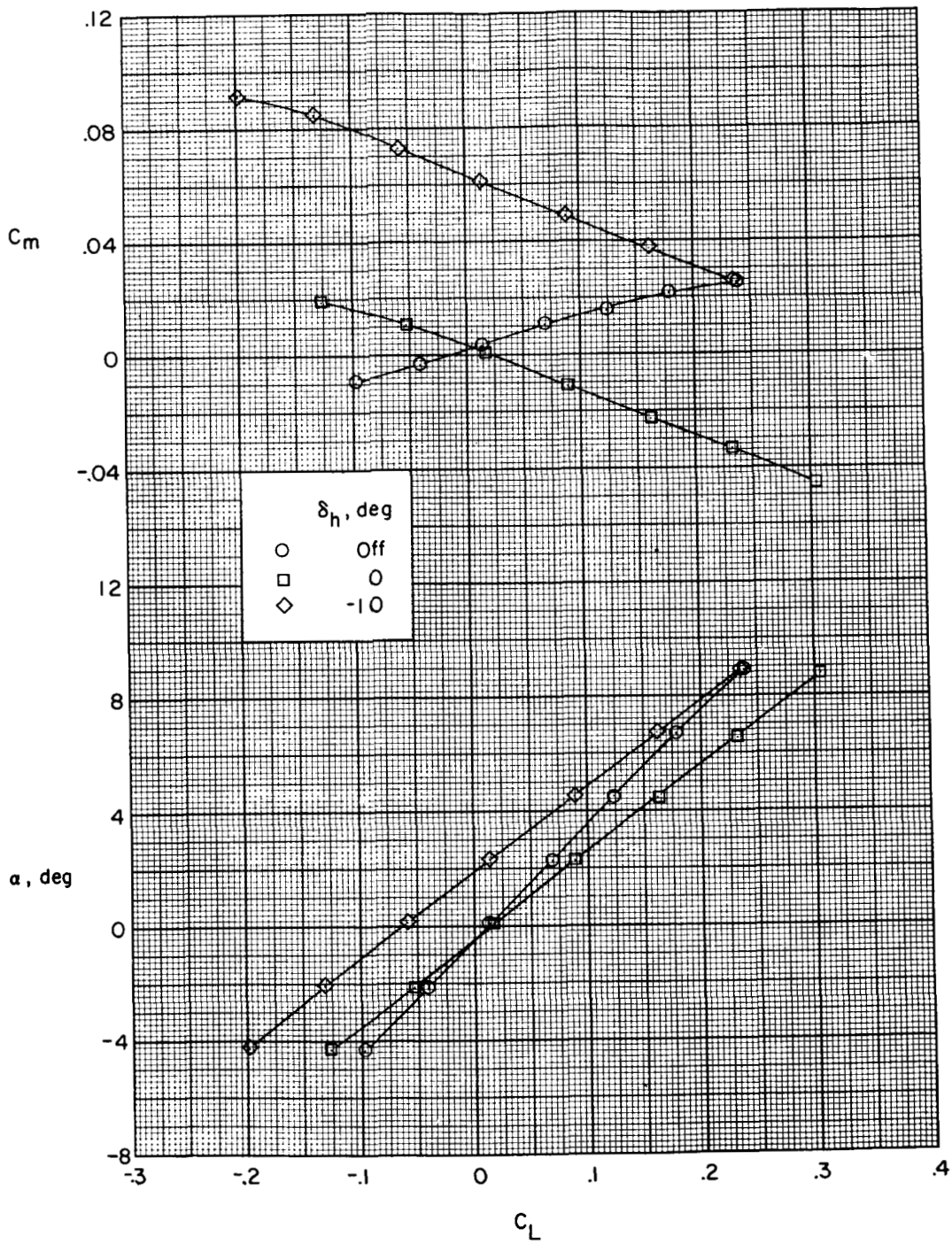

Figure 12.- Effect of horizontal-tail deflection on the aerodynamic characteristics in pitch; canard surface off; W_3BHV; $\Gamma = -20^\circ$.

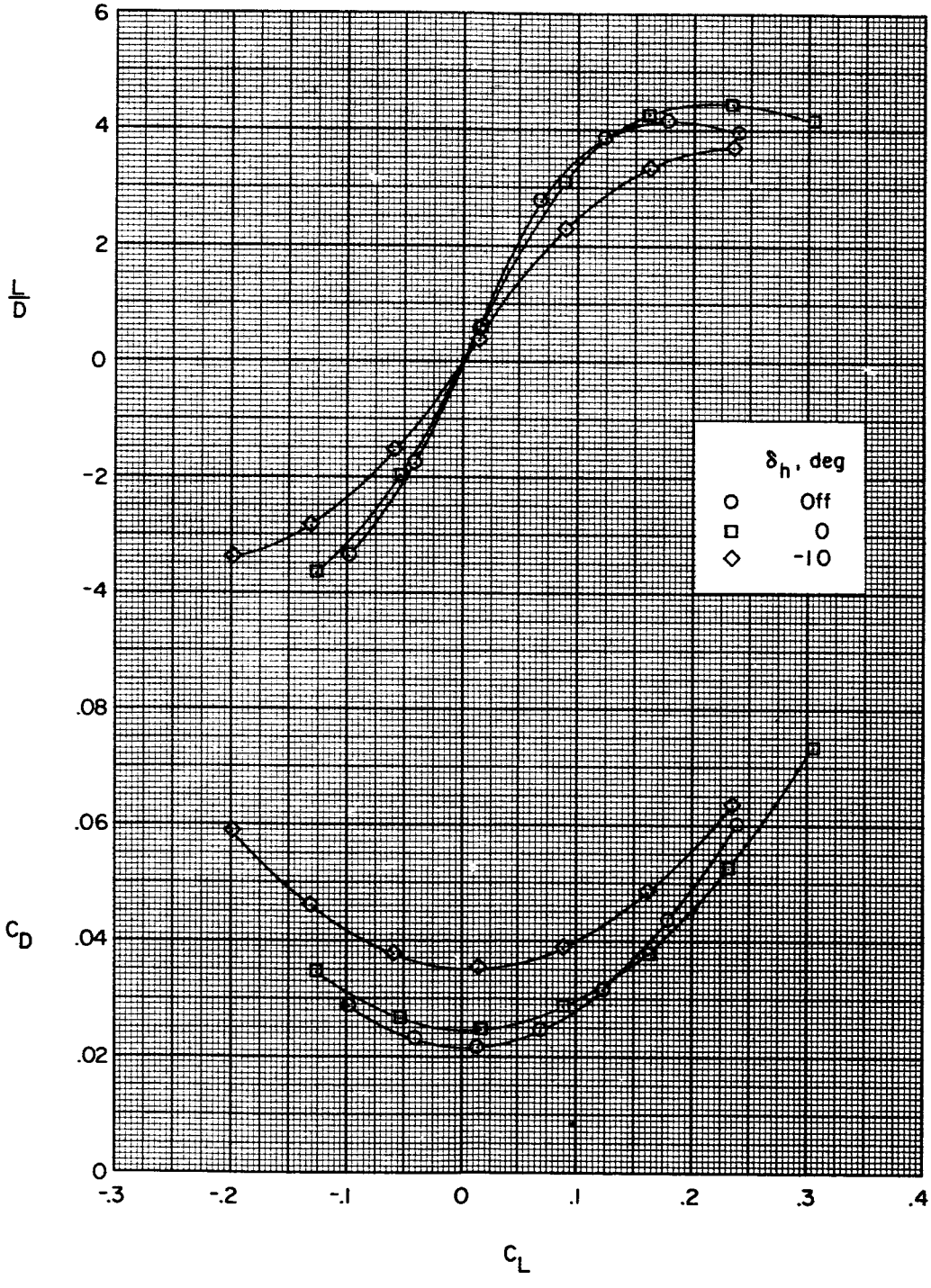

Figure 12.- Concluded.

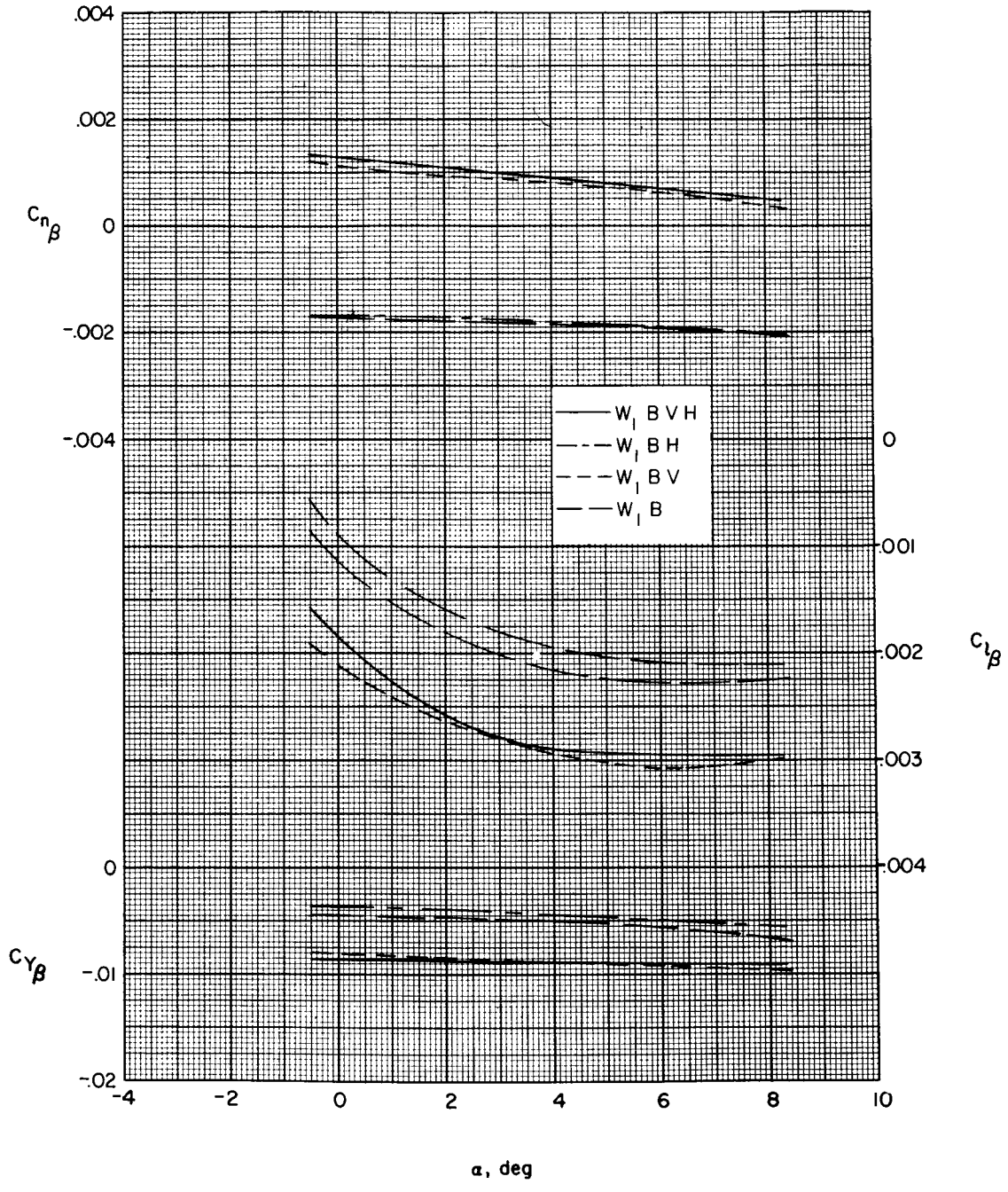

Figure 13.- Variation of sideslip derivatives with angle of attack for various combinations of components; wing 1; canard surface off; $\Gamma = 0^\circ$; $\delta_h = 0^\circ$.

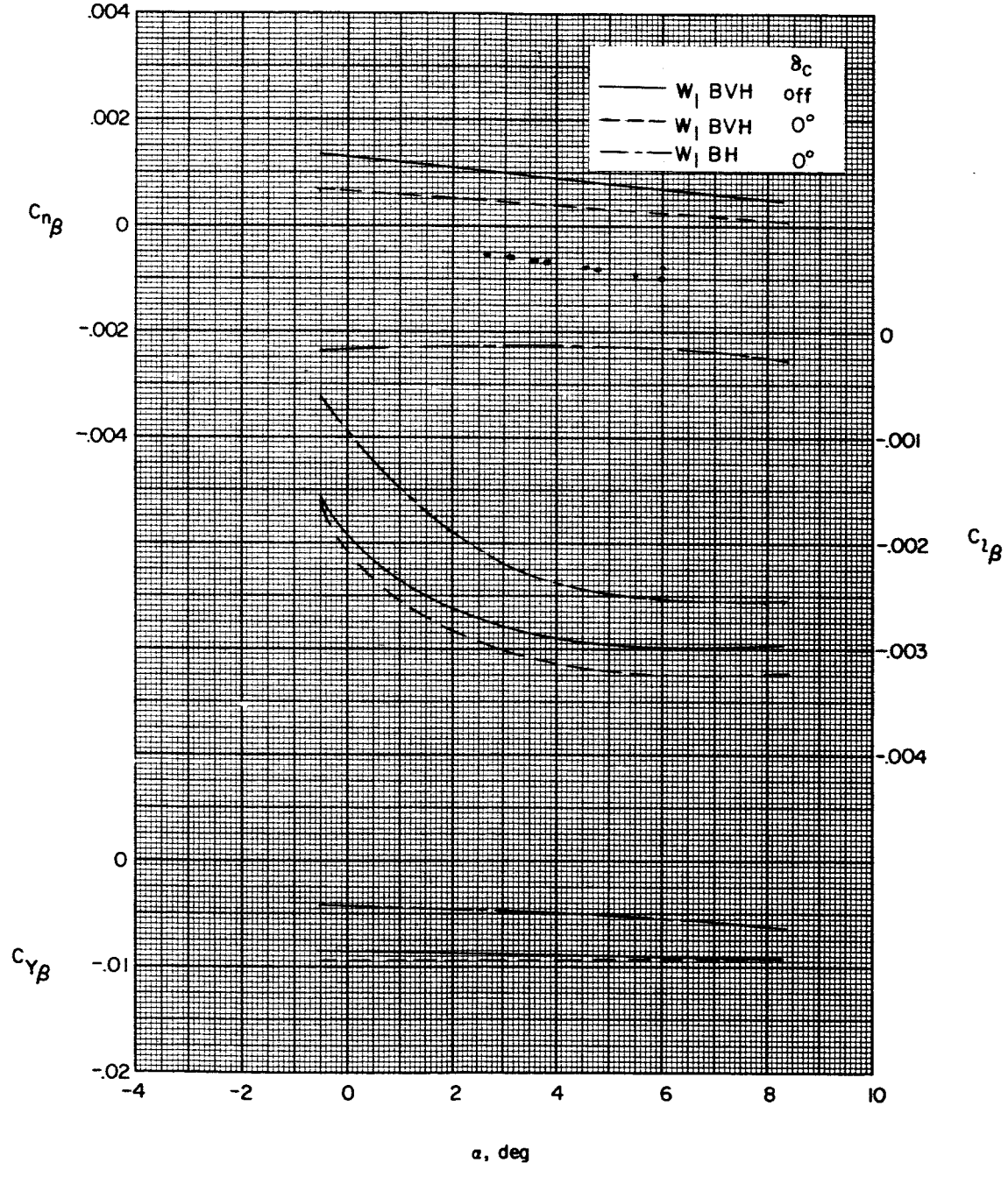

Figure 14.- Effect of canard surface and vertical tail on the sideslip derivatives; wing 1; $\Gamma = 0^{\circ}$; $\delta_h = 0^{\circ}$.

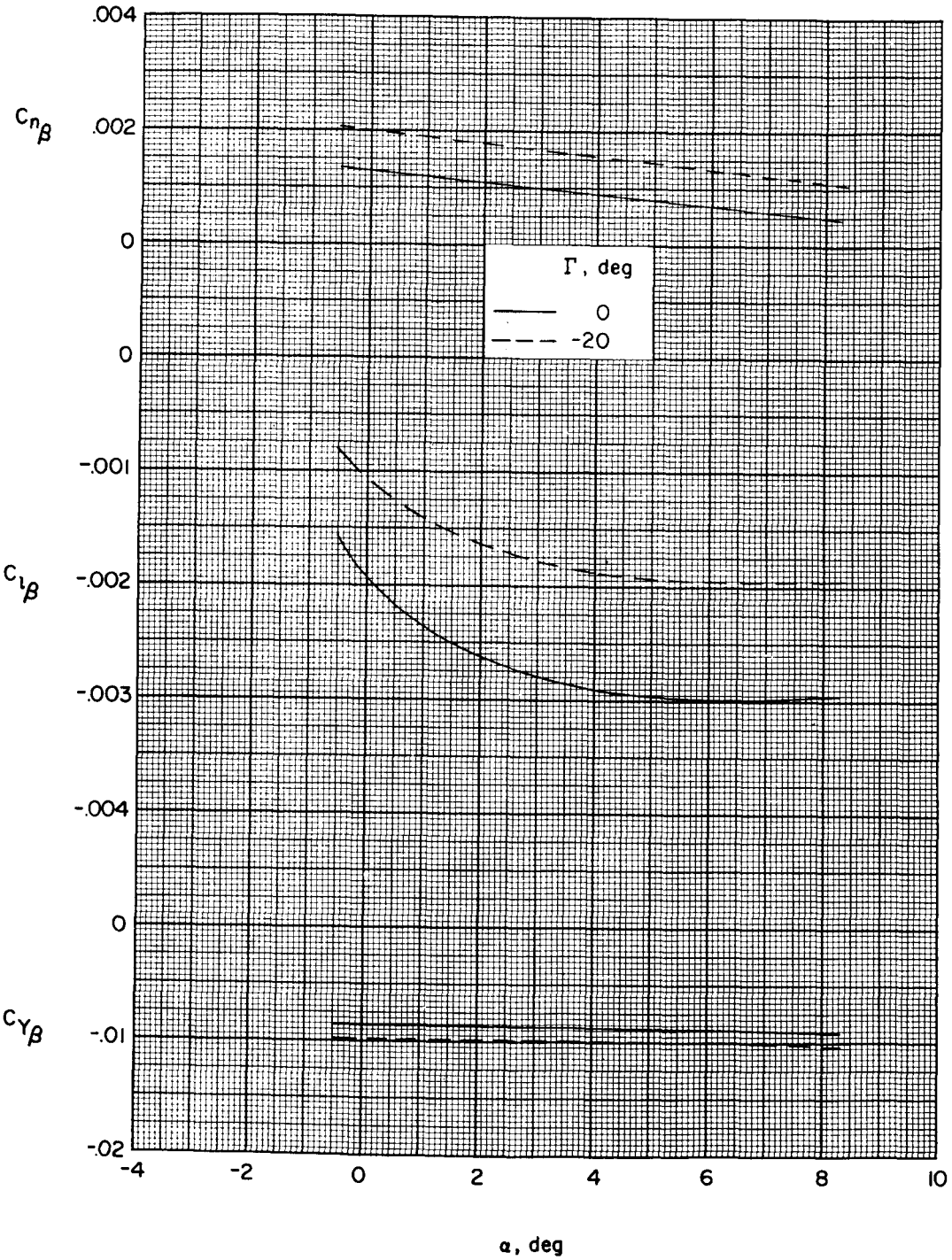

Figure 15.- Effect of horizontal-tail dihedral on the sideslip derivatives; wing 1; canard surface off; $\delta_h = 0^o$.

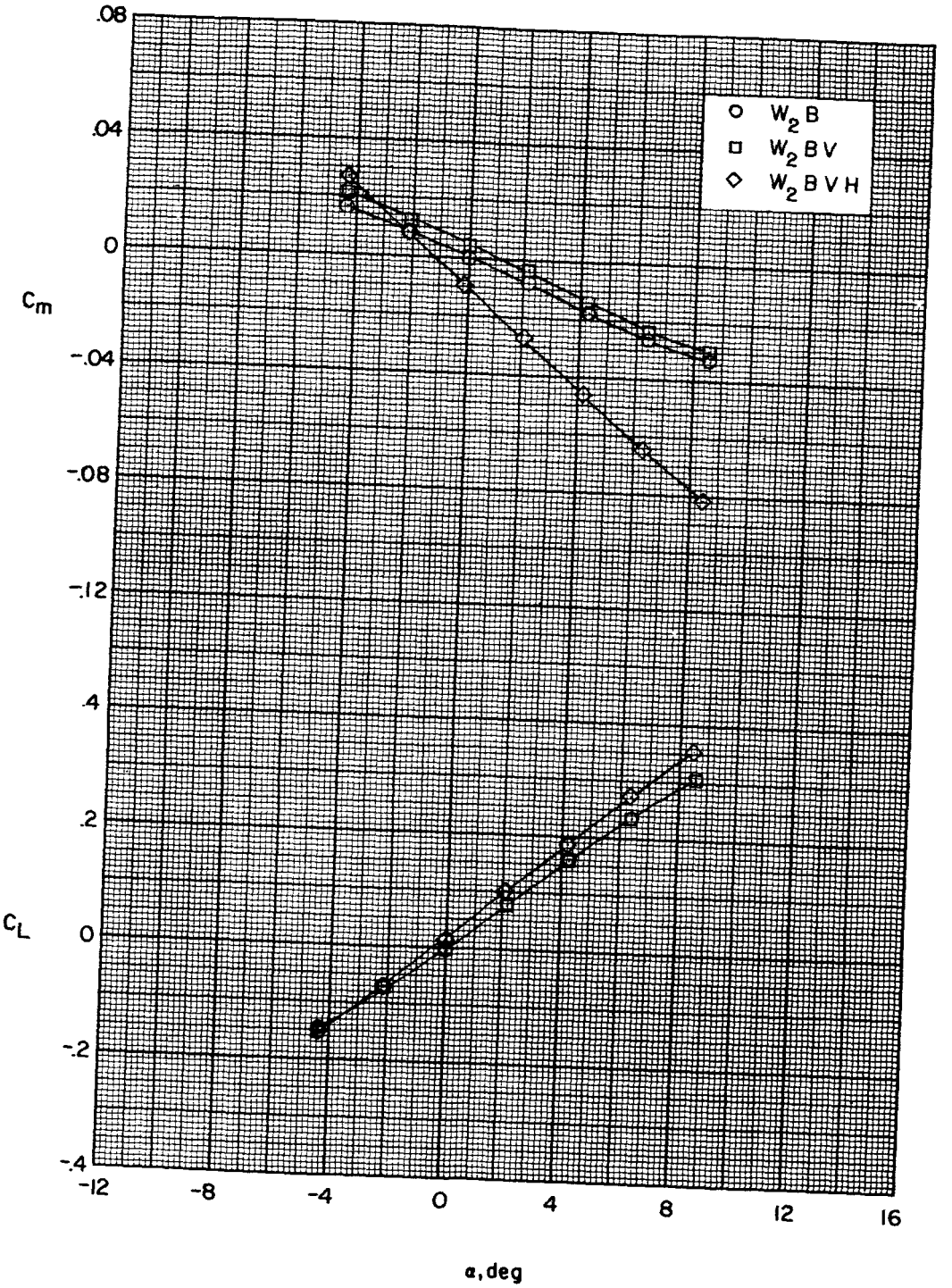

Figure 16.- Aerodynamic characteristics in pitch for various combinations of components; wing 2; canard surface off; $\Gamma = -20^{\circ}$.

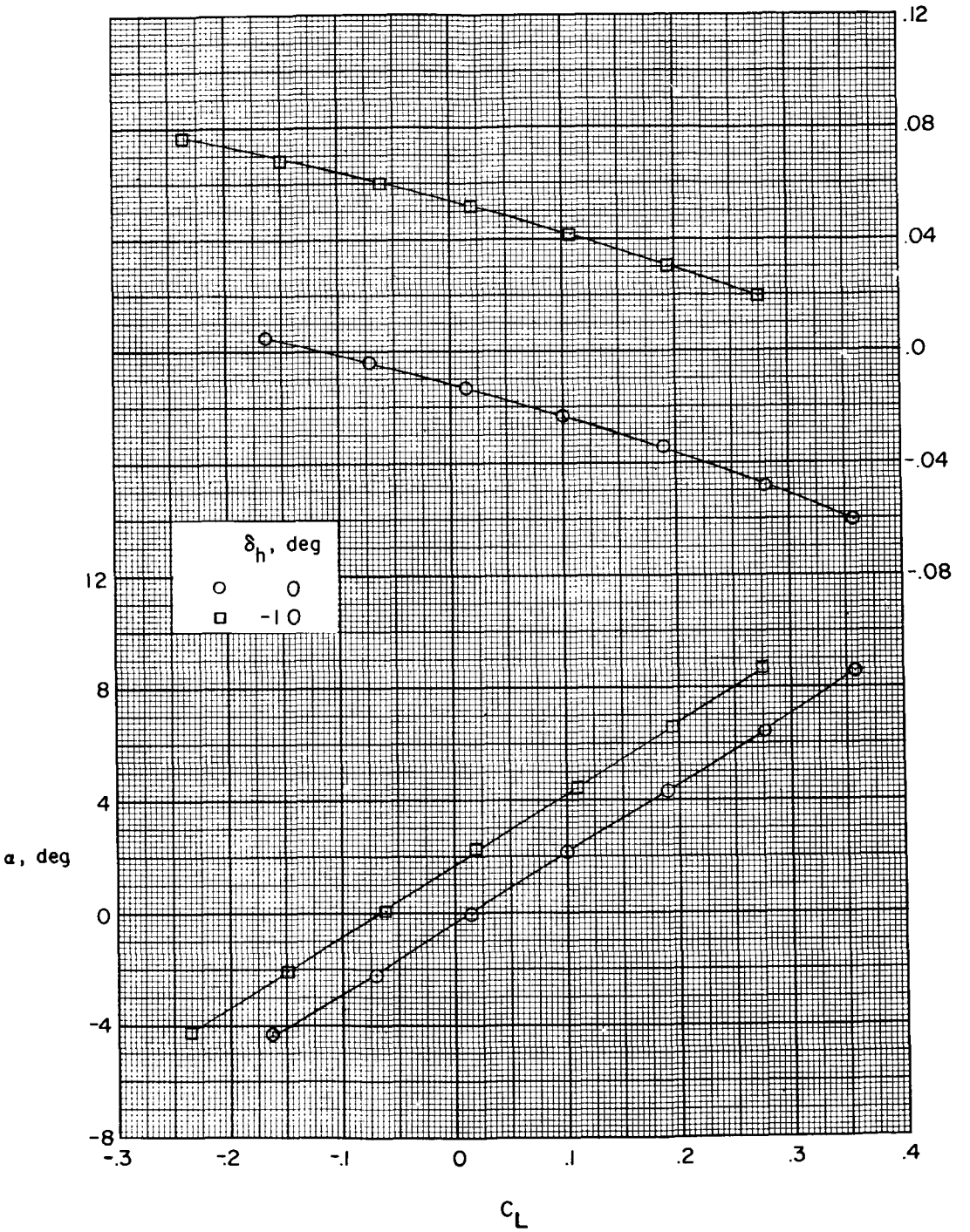

Figure 17.- Effect of horizontal-tail deflection on the aerodynamic characteristics in pitch; W_2BHVC; $\Gamma = -20^\circ$; $\delta_c = 0^\circ$.

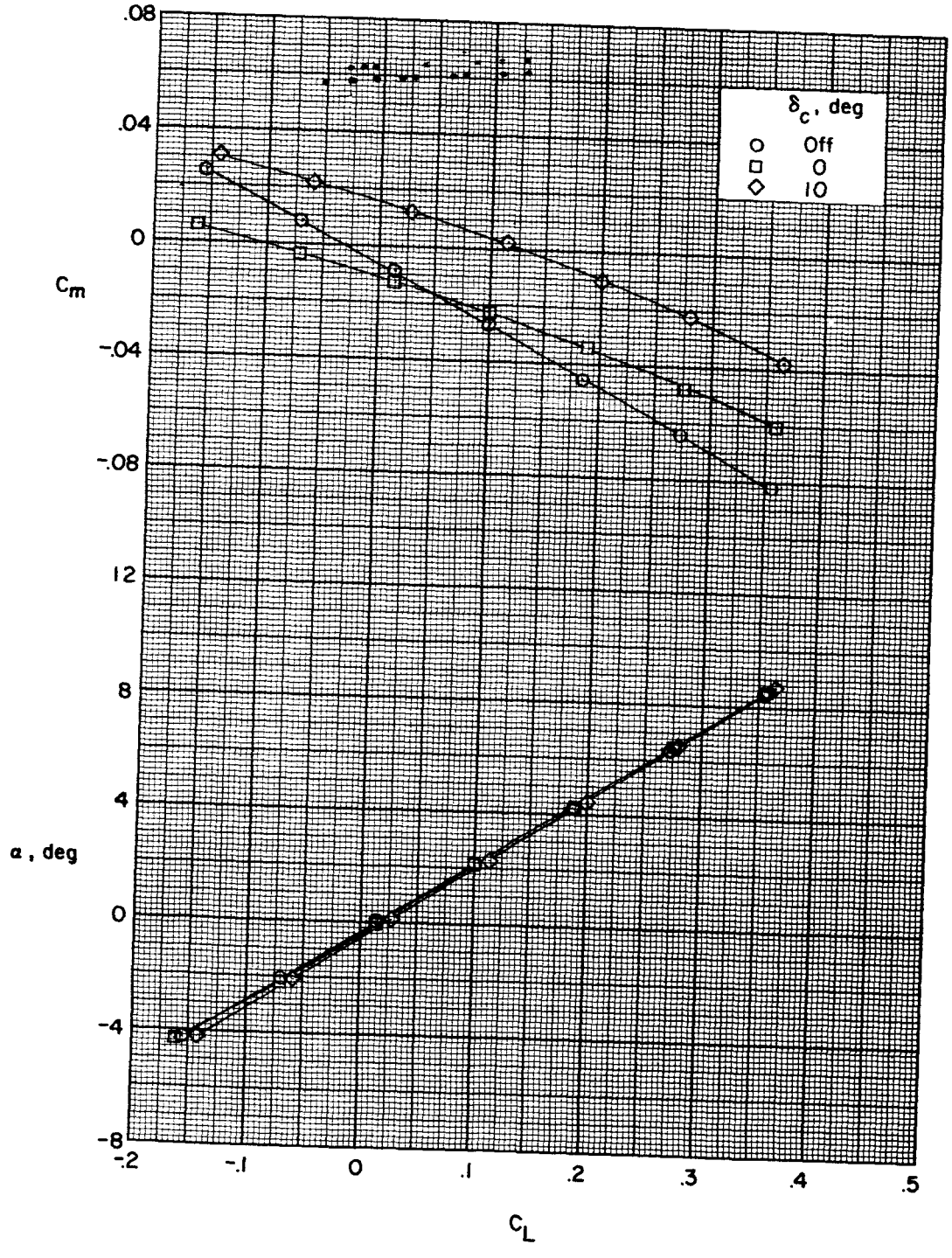

Figure 18.- Effect of canard-surface deflection on the aerodynamic characteristics in pitch; W_2BHVC; $\Gamma = -20^o$; $\delta_h = 0^o$.

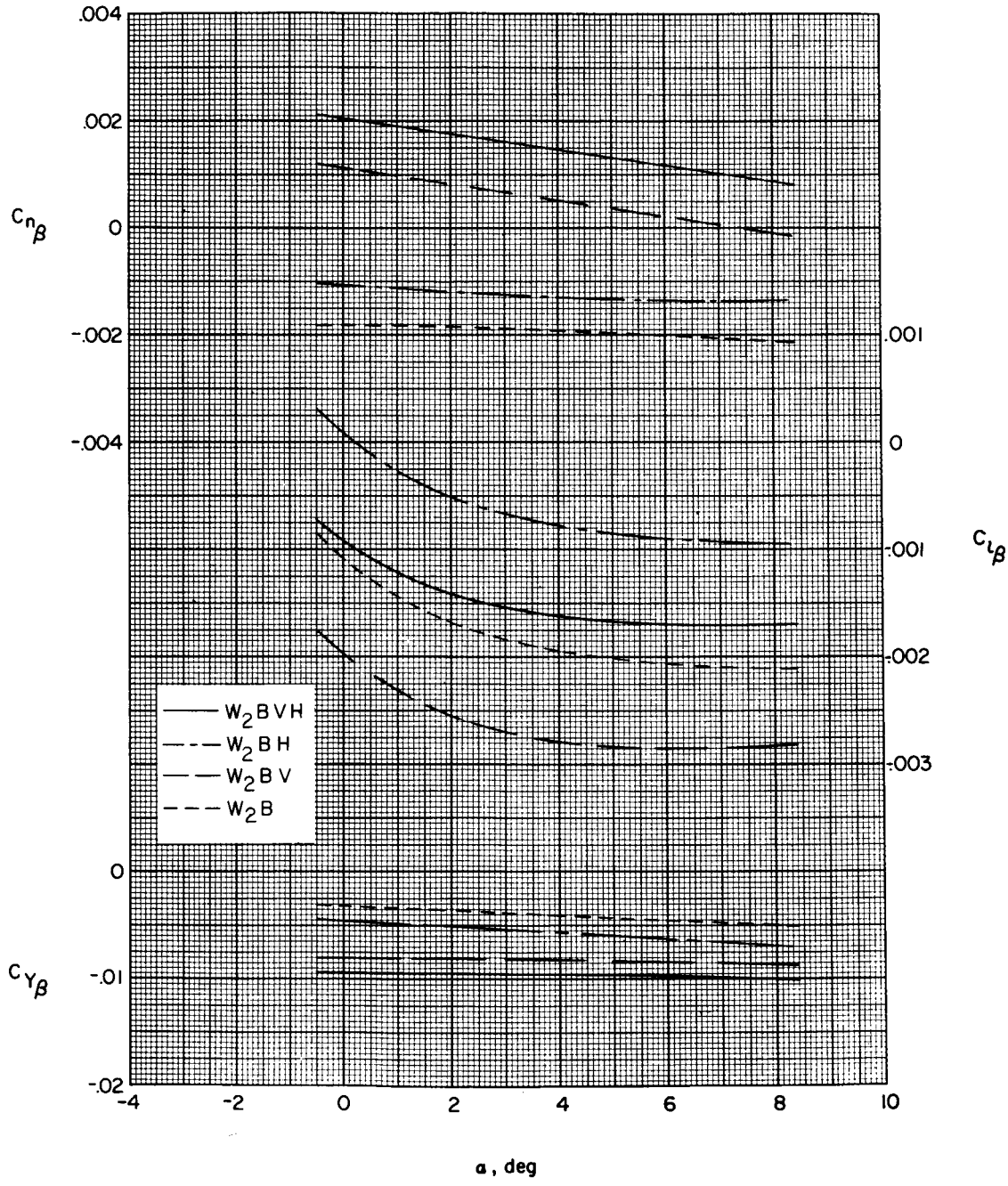

(a) Canard surface off.

Figure 19.- Variation of sideslip derivatives with angle of attack for various combinations of components; wing 2; $\Gamma = -20^\circ$; $\delta_h = 0^\circ$.

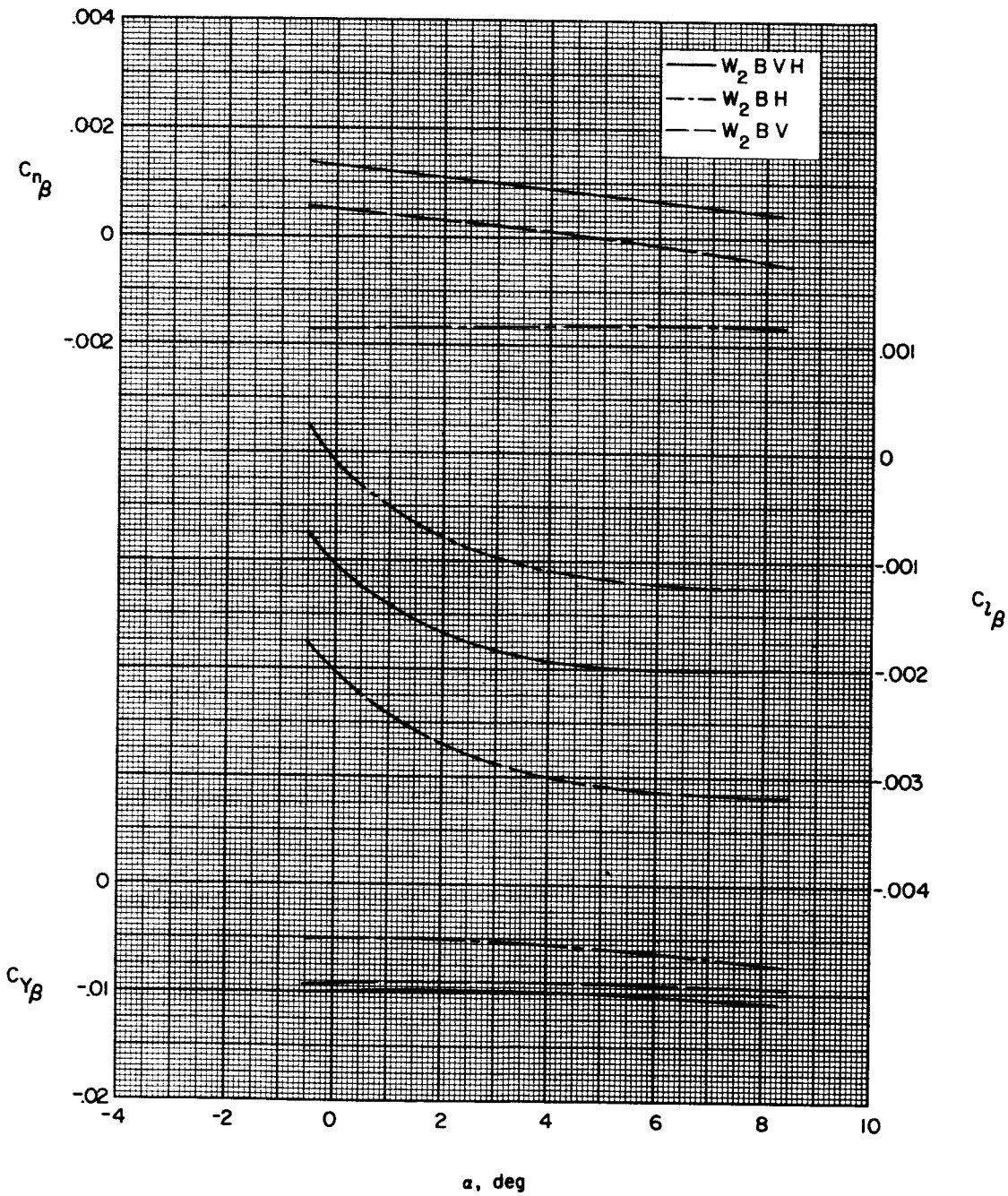

(b) Canard surface on ($\delta_c = 0^o$).

Figure 19.- Concluded.

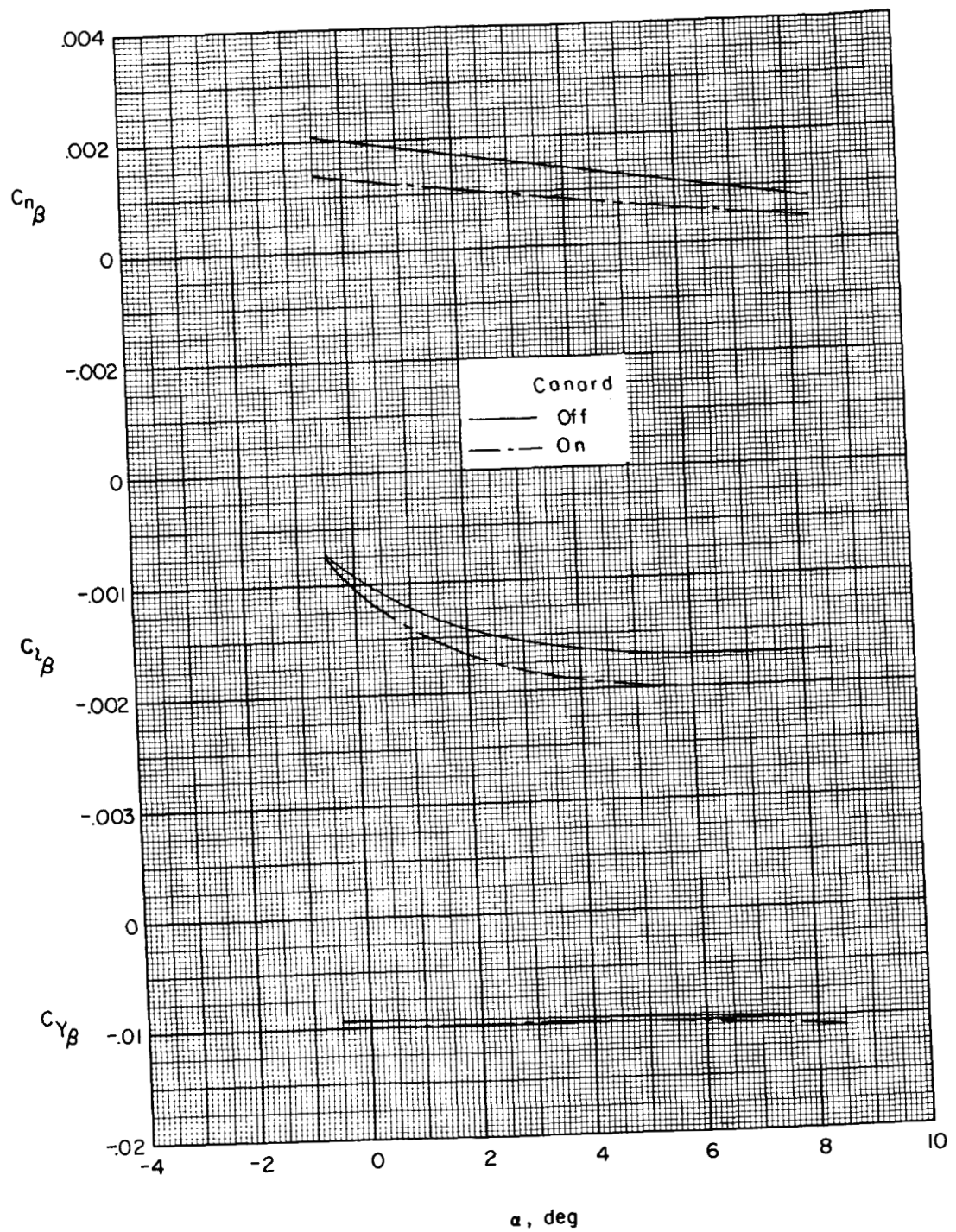

Figure 20.- Effect of canard surface on the sideslip derivatives; W_2BHV; $\Gamma = -20^\circ$; $\delta_h = 0^\circ$.

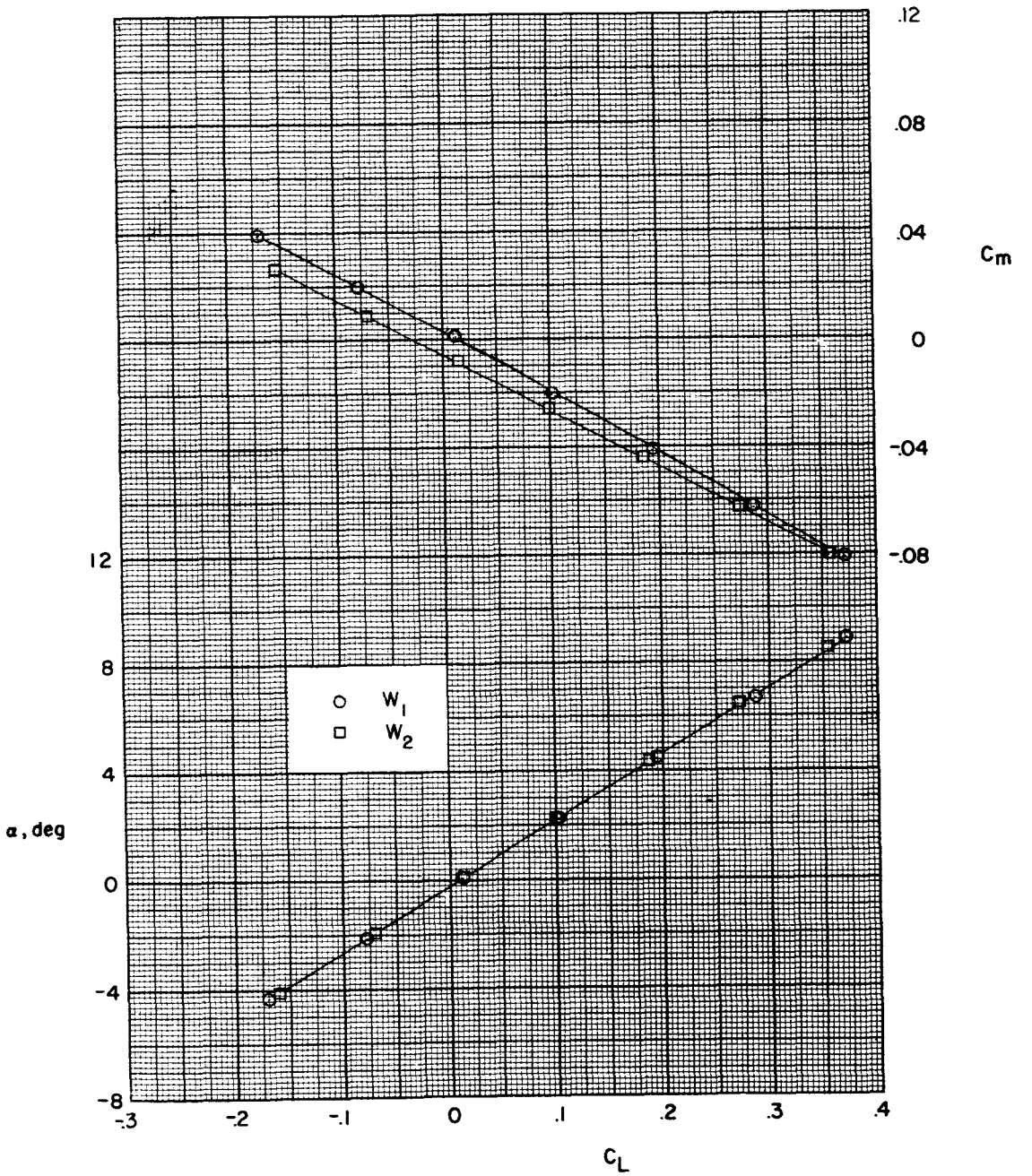

Figure 21.- Comparison of longitudinal aerodynamic characteristics of model with wings 1 and 2; canard surface off; $\Gamma = -20^{\circ}$; $\delta_h = 0^{\circ}$.